Necroptosis Signalling Promotes Inflammation, Airway Remodelling and Emphysema in COPD

Zhe Lu[1*], Hannelore P. Van Eeckhoutte[2*], Gang Liu[1,3], Prema M Nair[1], Bernadette Jones[1], Caitlin M. Gillis[3,4,5], B. Christina Nalkurthi[3], Fien Verhamme[2], Tamariche Buyle-Huybrecht[2], Peter Vandenabeele[4,5], Tom Vanden Berghe[4,5,6], Guy G. Brusselle[2], James M. Murphy[7], Peter A. Wark[1], Ken R. Bracke[2*], Michael Fricker[1*], Philip M. Hansbro[1,3*]

[1]Priority Research Centre for Healthy Lungs, Hunter Medical Research Institute, University of Newcastle, Newcastle, New South Wales, Australia; [2]Department of Respiratory Medicine, Laboratory for Translational Research in Obstructive Pulmonary Diseases, Ghent University Hospital, Ghent, Belgium; [3]Centre for Inflammation, Centenary Institute and University of Technology Sydney, Faculty of Science, Sydney, New South Wales, Australia; [4]VIB Center for Inflammation Research, Department for Biomedical Molecular Biology, Ghent University, Ghent, Belgium; [5]Methusalem program CEDAR-IC, Ghent University, B-9052 Ghent, Belgium; [6]Department Biomedical Sciences, University of Antwerp, Antwerp, Belgium; [7]Walter and Eliza Hall Institute of Medical Research and Department of Medical Biology, University of Melbourne, Victoria, Australia.

*These authors contributed equally to this manuscript.

Correspondence and requests for reprints should be addressed to Philip M. Hansbro, Ph.D., Centre for Inflammation, Centenary Institute and University of Technology Sydney, School of

AJRCCM Articles in Press. Published June 16, 2021 as 10.1164/rccm.202009-3442OC

Life Sciences, Faculty of Science, Sydney, New South Wales 2050, Australia. E-mail: philip.hansbro@uts.edu.au

Supported by grants and fellowships from the National Health and Medical Research Council of Australia (1175134, 1120252, 1099095, 1159582), the Australian Research Council (150102153), the University of Newcastle, the Hunter Medical Research Institute, University of Technology Sydney to P.M.H., IRIISS, Victorian Government Operational Infrastructure Support scheme to J.M.M., European Union Horizon 2020 Marie Skłodowska-Curie grant agreement No 796450 to C.M.G, Flemish grants (EOS MODEL-IDI, 30826052), FWO research grants (G.0E04.16N, G.0C76.18N, G.0B71.18N, G.0B96.20N), Methusalem (BOF16/MET_V/007), Foundation against Cancer (FAF-F/2016/865), CRIG and GIGG consortia, and VIB to P.V. Consortium of excellence focusing on inflammation (INFLA-MED) to T.V.B.

Author Contributions: Z.L., H.P.V.E, C.M.G., K.R.B., M.F. and P.M.H. designed and performed experiments and analyzed the data and G.L., J.M.M. and P.A.W. contributed. Z.L., H.P.V.E, K.R.B., M.F. and P.M.H. conceptualized studies and wrote the manuscript. H.P.V.E, C.M.G., F.V., T.B.H, P.V., T.V., G.G.B. and K.R.B. analyzed clinical data, assisted in performing experiments, helped analyze data and edited the manuscript, helped interpret data, and edited and revised the manuscript. K.R.B., M.F. and P.M.H. supervised studies and edited and revised the manuscript.

Running head: Necroptosis in COPD

Descriptor number: 9.13 COPD: Pathogenesis

Word count manuscript: 4,452, max 3,500

Word count abstract: 250, max 250

AJRCCM Articles in Press. Published June 16, 2021 as 10.1164/rccm.202009-3442OC

This article has an online data supplement, which is accessible from this issue's table of content online at www.atsjournals.org.

At a Glance

Scientific Knowledge on the Subject

Emphysema and COPD are likely underpinned by aberrant cell death that leads to airway inflammation and remodelling and emphysema. Apoptotic cell death can be programmed and controlled during apoptosis, whereas necroptosis defined by ruptured cell membranes is considered to be non-inflammatory, whereas necroptosis, a form of regulated necrosis, is highly pro-inflammatory. The roles of these pathways in COPD are poorly understood.

What the Study Adds to the Field

We used combination analysis of human COPD lung tissue, mouse models of experimental COPD, mice deficient in key necroptotic pathway mediators (RIPK3, MLKL) and inhibitors to define the roles of cell death pathways. Necroptotsis signalling is increased in the lungs in human and experimental COPD and correlate with disease severity. Genetic inhibition of necroptosis suppresses airway inflammation and remodelling and emphysema in experimental COPD, while pharmacological caspase inhibition reduces inflammation only. Inhibiting necroptosis may be a new therapeutic approach for COPD.

AJRCCM Articles in Press. Published June 16, 2021 as 10.1164/rccm.202009-3442OC

Abstract

Rationale: Necroptosis, mediated by RIPK3 and MLKL, is a form of regulated necrosis that can drive tissue inflammation and destruction, however its contribution to COPD pathogenesis is poorly understood.

Objectives: To determine the role of necroptosis in COPD.

Methods: Total and active (phosphorylated) RIPK3 and MLKL were measured in lung tissue of COPD patients and non-COPD controls. Necroptosis-related mRNA and proteins, and cell death were examined in lungs and pulmonary macrophages of mice with cigarette smoke (CS)-induced experimental COPD. Responses of *Ripk3*- and *Mlkl*-deficient ($^{-/-}$) mice and acute and chronic CS exposure were compared to wild-type mice. Combined inhibition of apoptosis (pan-caspase inhibitor qVD-OPh) and necroptosis (*Mlkl*$^{-/-}$ mice) was assessed.

Measurements and Main Results: Total MLKL protein in epithelium and macrophages, and pRIPK3 and pMLKL in lung tissue were increased in severe COPD compared to never smokers or smoker non-COPD controls. Necroptosis-related mRNA and protein levels were increased in lungs and macrophages in CS-exposed mice/experimental COPD. *Ripk3* or *Mlkl* deletion prevented airway inflammation upon acute CS-exposure. *Ripk3* deficiency reduced airway inflammation and remodelling and development of emphysematous pathology following chronic CS-exposure. *Mlkl* deletion and qVD-OPh treatment reduced chronic CS-induced airway inflammation, but only *Mlkl* deletion prevented airway remodelling and emphysema. *Ripk3* or *Mlkl* deletion and qVD-OPh treatment reduced CS-induced lung cell death.

AJRCCM Articles in Press. Published June 16, 2021 as 10.1164/rccm.202009-3442OC

Conclusions: Necroptosis is induced by CS exposure and increased in lungs of COPD patients and experimental COPD. Inhibiting necroptosis attenuates CS-induced airway inflammation, airway remodelling and emphysema. Targeted inhibition of necroptosis is a potential therapeutic strategy in COPD.

Keywords: COPD; Necroptosis; Apoptosis; RIPK3; MLKL; inflammation; remodelling; emphysema; macrophage; epithelium

AJRCCM Articles in Press. Published June 16, 2021 as 10.1164/rccm.202009-3442OC

COPD is a common lung disease characterised by persistent respiratory symptoms and impaired lung function (1). It is underpinned by a varied and complex set of pathologies, including airway inflammation, airway remodelling and emphysema (destruction and enlargement of alveoli). The major risk factor is exposure to cigarette smoke (CS). Inhaled corticosteroids combined with long-acting β2-agonists can partially suppress inflammation and provide symptomatic relief in COPD patients (1). However, there are currently no treatments that halt or reverse progression or disease or symptomatic burden, highlighting the need for mechanistic studies to identify new therapeutic targets.

Aberrant cell death correlates with the development of emphysema in COPD (2-4). Cell death can occur by apoptosis, various types of regulated necrosis or 'unregulated' necrosis. The mechanism by which cells die has important implications for inflammatory responses during disease (5). Apoptosis is the best characterized form of cell death and has been previously linked to increased lung cell death in emphysema (6). However, critical evidence of a causal relationship between apoptosis and emphysema is lacking, the role of apoptosis in COPD is poorly understood.

Necroptosis is a genetically encoded mechanism of necrotic cell death defined by rupture of the plasma membrane. It involves 4 RHIM domain-containing proteins including receptor interacting protein kinase (RIPK)-1 and -3, which eventually converge on RIPK3-mediated phosphorylation of MLKL, the executioner of necroptosis. It is a form of regulated cell death, but is highly pro-inflammatory due to the release of damage associated molecular patterns (DAMPs) into the extracellular environment following MLKL-mediated plasma membrane rupture (7). Selected Toll-like receptors (TLR) ligands, TNFα and IFNs can induce necroptosis, although the pathway is endogenously inhibited by pro-apoptotic caspase-8 (7, 8). These necroptosis stimuli are also implicated in COPD pathogenesis (9-11). Inhibiting RIPK1

AJRCCM Articles in Press. Published June 16, 2021 as 10.1164/rccm.202009-3442OC

kinase activity can prevent cell death by apoptosis and/or necroptosis. In the latter, RIPK1 is an upstream activator of RIPK3 and MLKL leading to necroptosis. RIPK1 inhibition can suppress airway inflammation induced by acute CS exposure, and prevent decreases in metabolic activity of epithelial cell cultures induced by toxic doses of CS extract (CSE) *in vitro* (12). However, the role of RIPK3 and MLKL and the relative contributions of necroptosis and apoptosis in COPD pathogenesis have not been assessed.

Here, we define for the first time the contribution of necroptosis- and apoptosis-related signalling to COPD pathogenesis, using lung tissue samples from patients with COPD, never smokers and smoker non-COPD controls, and mouse models of CS-induced experimental COPD. Some of the results of these studies have been previously reported in the form of an abstract (13-15).

Methods

Human and mouse ethics statements and studies, induction of CS-induced experimental COPD, qVD-OPh intervention, BALF staining, Immunohistochemistry and immunofluorescence, RNA-sequencing of FACS sorted alveolar macrophages and data processing, and Statistical analysis

Detailed descriptions of these are as previously described and are in the online supplement (16-44).

Human ethics

Human studies were approved by the medical ethics committee of Ghent University Hospital (2016/0132) and University Hospital Gasthuisberg (S51577). Descriptions of the study cohorts and sampling are in the supplement (Tables E1 and E2).

AJRCCM Articles in Press. Published June 16, 2021 as 10.1164/rccm.202009-3442OC

Human lung samples

Lung tissues from our biobank at Ghent University Hospital and explants from end-stage COPD patients from UZ Gasthuisberg Leuven, Belgium were analyzed. Based on pre-operative spirometry, diffusion capacity tests and questionnaires, subjects were categorized as never-smokers and smokers without airflow limitation or patients with COPD. COPD severity was defined according to the Global Initiative for Chronic Obstructive Lung Disease (GOLD) classification. No patients were treated with neo-adjuvant chemotherapy. Lung tissue from patients with solitary pulmonary tumors was obtained at the maximum distance from the pulmonary lesions and without signs of retro-obstructive pneumonia or tumor invasion by a pathologist.

Animal ethics

Mouse studies were approved by the University of Newcastle Animal Ethics Committee, and the Faculty of Medicine and Health Sciences (Ghent University).

Experimental COPD

In Hunter Medical Research Institute, mice were exposed to cigarette smoke (CS) by a custom-built nose-only system, 12 cigarettes per run, twice/day, 5 days/week for up to 8 weeks (12-20). In Ghent University (alveolar macrophage RNAseq), mice were exposed whole body to the smoke of five cigarettes without filter 4 times/day, 5 days/week, for 4 weeks (21-24). Control mice were exposed to normal air.

Statistical analysis

For human studies, data are presented as median±interquartile range (IQR), (n=8-16 per group). The Shapiro-Wilk test was used to assess normality, followed by one-way ANOVA with

AJRCCM Articles in Press. Published June 16, 2021 as 10.1164/rccm.202009-3442OC

Bonferroni *post-hoc* for multiple comparisons or Kruskal-Wallis test with Dunn's multiple comparisons. Spearman rank correlation was used to test for correlations with $p<0.05$ considered significant. Linear regression analyses were performed using SPSS to correct for potential confounders (age, sex, current smoking). For mouse experiments, data are presented as mean ± standard error of the mean (SEM) and n=4-6 mice per group. Students t-tests were performed to compare 2 groups and for multiple comparisons of more than 2 groups Bonferroni corrections were done.

Results

Levels and activation of RIPK3 and MLKL in lung resections from COPD patients

We performed immunohistochemical staining for total RIPK3 and MLKL and immunoblotting for total and phosphorylated (p)RIPK3 and pMLKL on lung tissue from two cohorts (clinical characteristics in Supplemental Tables E1 and E2), comparing never-smokers and smokers without airflow obstruction and COPD GOLD stage II and III-IV participants. Immunohistochemistry revealed positive RIPK3 and MLKL staining in the airway epithelium (Figure 1A and *see* Figure E1A). Quantification of epithelial RIPK3 (*see* Figure E1B) and immunoblot analysis for total RIPK3 and MLKL (*see* Figures E1C-F), showed no differences in total RIPK3 or MLKL across the different patient groups. Quantification of epithelial MLKL showed significantly higher levels in GOLD stage III-IV patients compared to never-smokers and smokers without airflow limitation (Figure 1B), which remained significant after adjustment for age, gender and smoking status (β 13.7±5.9, $p=0.0251$). We also detected MLKL protein in alveolar macrophages (Figure 1C) and observed a significant increase in MLKL staining intensity in alveolar macrophages of COPD GOLD III-IV patients versus never-smokers (Figure 1D). pRIPK3 and pMLKL were significantly increased in lung tissue homogenates from severe to very severe COPD (GOLD stage III-IV) patient compared to

AJRCCM Articles in Press. Published June 16, 2021 as 10.1164/rccm.202009-3442OC

smokers without airflow limitation (Figure 1E-H, when normalized to GAPDH or Figure E1G-H, when normalized to total RIPK3 or MLKL protein). After adjustment for age, gender and current smoking by linear regression analyses, the associations for pRIPK3 (β 0.90±0.42, p=0.038) and pMLKL protein levels (β 1.58±0.46, p=0.002) with COPD GOLD III-IV remained significant. Moreover, we found a strong, positive correlation between pRIPK3 and pMLKL protein levels (Figure 1I, Rs=0.7287, p=0.0007). pRIPK3 and pMLKL protein levels had a significant negative correlation with the diffusing lung capacity for carbon monoxide (DL_{CO}, Figure 1J and 1K, Rs=-0.5493, p=0.0004 and Rs=-0.5470, p=0.0004). Thus, elevated expression and activation of necroptosis proteins are associated with increasing COPD severity.

Upregulation of necroptosis-related mRNA and proteins in the lung in experimental COPD

To assess the potential role of necroptosis in COPD pathogenesis, we employed both nose-only (1-, 4-, 8- or 12-weeks exposure) and whole body (4-weeks exposure) mouse models of CS-induced lung inflammation and COPD-like pathology. We performed TUNEL staining to assess cell death and found an increase in positive cells in the lungs in the airways, parenchyma and immune cells but were not more prominent in experimental COPD but were not more prominent in a particular cell type (8 and 12 weeks, Figure 2A). We next examined the mRNA transcript levels of core necroptosis-related factors *Ripk1*, *Ripk3* and *Mlkl* through qPCR of whole lung tissue from mice exposed to CS at timepoints that preceded (4 weeks) and were concomitant with (8 and 12 weeks) increased cell death (TUNEL staining) in the lung parenchyma. *Ripk1* mRNA expression was upregulated at 4 weeks but not 8 or 12 weeks of nose-only CS exposure (*see* Figures E2A-C) while *Ripk3* mRNA was not differentially expressed in whole lungs (*see* Figures E2D-F) compared to normal air-exposed mice. *Mlkl* mRNA was partially increased at 4 weeks (Figure 2B) and was significantly increased at 8 and

AJRCCM Articles in Press. Published June 16, 2021 as 10.1164/rccm.202009-3442OC

12 (p=0.0644) weeks of CS exposure (Figure 2C). qPCR comparison of blunt dissected airway *versus* parenchymal tissue revealed increased airway mRNA expression of *Mlkl* after 8 weeks of CS exposure (Figure 2E). RNA-sequencing of alveolar macrophages sorted by flow cytometry from BALF of mice exposed to whole body CS for 4 weeks revealed significant increases in *Ripk3* and *Mlkl* but not *Ripk1* mRNA compared to normal air-exposed controls (Figures 2F-H). Ripk1 and Ripk3 protein levels were significantly increased after 8 weeks of nose-only CS-exposure, when emphysematous pathology has developed (Figure 2I-K) (17). Immunoblot analysis of total Mlkl protein in lungs of 8-week CS- and air-exposed mice revealed two bands, the lower of which (~50 kDa) corresponds to Mlkl protein which was also based on the absence of staining in lung tissue from *Mlkl*-deficient ($^{-/-}$) mice (Figures 2L and 2M). Mlkl protein was increased in the lungs of 8-week CS-exposed mice. Similar to human COPD, immunofluorescence staining revealed increased MLKL intensity in airway epithelial cells and macrophages of CS-exposed mice (8 weeks), which was significantly elevated in macrophages (Figure 2N and *see* Figures E2G and E2H). Thus, core necrosome components particularly, Mlkl were increased at mRNA and protein levels in lung tissue and alveolar macrophages in experimental COPD, similar to that observed in airways and alveolar macrophages in human samples.

RIPK3 and MLKL drive airway inflammation in response to acute CS-exposure

Ripk3$^{-/-}$, *Mlkl*$^{-/-}$ and wild-type (WT) mice were exposed to nose-only CS or normal air for 4-days. On day 5, BALF was collected and total and differential leukocytes were enumerated (Figure 3). The numbers of total leukocytes, macrophages, neutrophils and lymphocytes in BALF significantly increased after CS exposure in *Ripk3*$^{-/-}$, *Mlkl*$^{-/-}$ and WT groups (Figure 3A-H). However, the numbers of total leukocytes and neutrophils were significantly reduced in CS-exposed *Ripk3*$^{-/-}$ and *Mlkl*$^{-/-}$ mice compared to WT controls (Figures 3A, 3C, 3E and 3G).

AJRCCM Articles in Press. Published June 16, 2021 as 10.1164/rccm.202009-3442OC

Airway macrophage numbers tended to be lower in *Ripk3*$^{-/-}$ and *Mlkl*$^{-/-}$ mice (Figure 3B), and lymphocytes were significantly reduced in CS-exposed *Ripk3*$^{-/-}$ compared to WT mice, with a similar trend observed in *Mlkl*$^{-/-}$ mice (Figure 3D). To further evaluate whether RIPK3 and MLKL deficiency affected acute CS-induced pulmonary inflammation, qPCR was used to assess the mRNA expression of pro-inflammatory factors in whole lung tissues of mice after 1 week of nose-only CS exposure. Transcript levels of *Cxcl1*, *Mmp8*, *Mmp12*, *Ym1*, *Marco* and *Mip1a* all increased after CS- compared to air-exposure in WT mice *(see* Figures E3A-M). *Mlkl* deficiency prevented the increase in *Cxcl1*, *Mmp12*, *Ym1* and *Marco*, with some similar trends observed in *Ripk3*$^{-/-}$ mice. *Mlkl* mRNA was significantly increased in WT mice (*see* Figure E3N). There was no detectable expression of *Ripk3* or *Mlkl* mRNA in lung tissue from respective deficient mice, confirming their deletion *(see* Figures E3G and E3N).

Ripk3 deficiency reduces airway inflammation, airway remodelling and emphysema in experimental COPD

To examine the role of Ripk3 in inflammation and pathology in experimental COPD, we exposed *Ripk3*$^{-/-}$ and WT mice to nose-only CS for 8 weeks. The numbers of total leukocytes, macrophages, neutrophil and lymphocytes in BALF were significantly increased after CS exposure in WT mice (Figure 4A-D). *Ripk3* deficiency prevented CS-induced increases in total BALF leukocytes, macrophages and lymphocytes, with a trend towards decreased neutrophils compared to WT. mRNA expression of *Cxcl1*, *Mmp8*, *Mmp12*, *Ym1*, *Marco* and *Mip1a* all increased after CS exposure in WT groups *(see* Figure E4). *Ripk3* deficiency suppressed the increases in *Ym1* and *Marco* mRNA in CS- compared to WT CS-exposed controls but did not affect the expression of other factors. CS exposure significantly increased histopathology scores in both airway and large peribronchial blood vessels in both genotypes, however, *Ripk3*$^{-/-}$ mice had significantly less airway inflammation compared to WT counterparts with a similar

AJRCCM Articles in Press. Published June 16, 2021 as 10.1164/rccm.202009-3442OC

trend towards decreased perivascular inflammation (Figures 4E and 4F). Alveolar macrophage numbers were significantly increased with CS exposure in WT mice and were significantly reduced in *Ripk3*$^{-/-}$ mice (Figure 4G). CS exposure of WT mice significantly increased collagen deposition around the airways, which was attenuated in the absence of Ripk3 (Figures 4H and 4I). CS-induced epithelial thickening was also significantly reduced in *Ripk3*$^{-/-}$ mice compared to WT (Figure 4J). CS exposure increased mean linear intercept (MLI) in WT mice which was significantly reduced in *Ripk3*$^{-/-}$ mice, indicating the attenuation of emphysematous pathology. (Figures 4K and 4L).

Both *Mlkl* deficiency and pan-caspase inhibition reduce chronic CS-induced airway inflammation

RIPK3 has additional functions in inflammatory cytokine production and apoptosis, while MLKL has only been reliably attributed functions in necroptosis (45, 46) . Thus, to examine whether the effects of RIPK3 loss could be attributed exclusively to necroptosis-deficiency, we examined disease features of *Mlkl-/-* relative to WT mice in experimental COPD. In addition, to assess the role of apoptosis and investigate the potential of combined inhibition of apoptotic and necroptotic cell death pathways in COPD, some WT groups were treated with pan-caspase inhibitor qVD-OPh or vehicle. The numbers of total leukocytes in BALF significantly increased after CS exposure in vehicle-treated WT mice, but not in vehicle-treated *Mlkl*$^{-/-}$ or qVD-OPh treated WT or *Mlkl*$^{-/-}$ mice (Figure 5A). This reduction in total leukocytes appeared to be specifically driven by significant inhibition of airway macrophage and neutrophil accumulation, while lymphocytes accumulated in high numbers in CS *versus* air-exposed *Mlkl*$^{-/-}$ qVD-OPh treated mice, albeit at lower numbers than macrophages or neutrophils (Figures 5B-D). Treatment of *Mlkl*$^{-/-}$ mice with qVD-OPh resulted in similar decreases in CS-induced BALF cellular inflammation compared to *Mlkl* deficiency or qVD-OPh of WT mice. *Cxcl1*,

AJRCCM Articles in Press. Published June 16, 2021 as 10.1164/rccm.202009-3442OC

Mmp8, *Mmp12* and *Ym1* mRNA expression significantly increased after CS exposure in vehicle-treated WT mice and levels of expression were significantly reduced in vehicle-treated *Mlkl*$^{-/-}$ and qVD-OPh treated WT or *Mlkl*$^{-/-}$ mice (Figure E5). *Marco* mRNA expression was significantly increased in all groups after CS exposure but was reduced in qVD-OPh-treated WT mice (Figure E5E). *Mip1a* mRNA expression was also significantly increased after CS exposure only in vehicle-treated WT mice and levels of expression were significantly lower in qVD-OPh treated WT and *Mlkl*$^{-/-}$ mice (Figure E5F). Mlkl was significantly induced in CS-exposed WT vehicle-treated treated mice. qVD-OPh treatment partially reduced CS-induced *Mlkl* mRNA expression in WT mice (*see* Figure E5G).

Differential effects of *Mlkl* deficiency *versus* caspase inhibition on experimental COPD pathology

To examine the impact of inhibiting apoptosis and/or necroptosis on lung pathology in experimental COPD, we performed histopathological analysis (Figures 6A and 6B). In the airways, CS exposure induced inflammation in all groups compared to normal air-exposed controls (Figure 6C). However, histopathology score was significantly reduced in both CS-exposed vehicle-treated *Mlkl*$^{-/-}$ or qVD-OPh treated WT or *Mlkl*$^{-/-}$ mice, compared to vehicle-treated WT controls. Similarly, perivascular inflammation also increased after CS exposure in all groups but was significantly reduced in qVD-OPh treated WT and *Mlkl*$^{-/-}$ mice compared to vehicle-treated WT mice (Figure 6D). There were significantly fewer parenchymal macrophages in CS-exposed *Mlkl*$^{-/-}$ mice compared to their WT counterparts with or without qVD-OPh treatment (Figure 6E). CS exposure induced collagen deposition in vehicle-treated WT mice, but this was prevented in *Mlkl*$^{-/-}$ mice, irrespective of qVD-OPh treatment (Figure 6F). Similarly, epithelial thickness was increased in CS-exposed WT but not *Mlkl*$^{-/-}$ mice, irrespective of qVD-OPh treatment (Figure 6G). MLI significantly increased in CS-exposed

AJRCCM Articles in Press. Published June 16, 2021 as 10.1164/rccm.202009-3442OC

WT mice irrespective of vehicle/qVD-OPh treatment, whilst *Mlkl*$^{-/-}$ mice did not develop emphysema in any experimental condition (Figure 6H).

Ripk3 and *Mlkl* deficiency and qVD-OPh treatment protect from CS-induced lung cell death in experimental COPD

TUNEL staining for total apoptotic and necrotic cell death and active caspase-3 staining for apoptosis was performed on sequential formalin-fixed lung sections of mice exposed to CS or normal air for 8 weeks. Both TUNEL-positive and active (cleaved) caspase-3-positive cells increased in CS-exposed compared to air-exposed groups (Figures 7A-D). *Ripk3* deficiency attenuated CS-induced increases in TUNEL-positive and active caspase-3-positive cells compared to WT mice (Figures 7A and 7B). Similarly, *Mlkl* deficiency and/or qVD-OPh treatment reduced CS-induced increases in TUNEL-positive events (Figure 7C) and prevented CS-induced increases in active caspase-3 staining that was only observed in the WT vehicle-treated group (Figure 7D).

Discussion

Here we describe the dysregulation and activation of the core necrosome components RIPK3 and MLKL in clinical COPD lung tissue samples, and demonstrate similar upregulation of necroptosis-related signalling in CS-induced experimental COPD. Through a combination of genetic deletion of core necrosome components (RIPK3 and MLKL) and pan-caspase inhibition to prevent apoptosis, we define for the first time the differential contributions of necroptosis *versus* apoptosis signalling to key pathologies in experimental COPD. This highlights potential roles for regulated necrosis, particularly necroptosis, in COPD pathogenesis, and suggests regulation of necroptosis represents a novel therapeutic target in COPD.

AJRCCM Articles in Press. Published June 16, 2021 as 10.1164/rccm.202009-3442OC

We profiled necroptosis signalling components RIPK3 and MLKL in lung tissue samples from COPD and non-COPD controls. We found that MLKL, the critical membrane-disrupting executioner of necroptotic cell death was increased in the bronchial epithelium and alveolar macrophages in severe COPD patients *versus* controls. During necroptosis initiation, MLKL becomes phosphorylated by RIPK3, which is required to trigger a conformational change allowing plasma membrane translocation, oligomerization and membrane disruption resulting in membrane leakage, rupture and necrotic cell death (6). Critically, phosphorylated RIPK3 and MLKL were elevated in lung tissues of severe COPD patients, which remained significant after adjustment for age, gender and current smoking. Moreover, we found a strong positive correlation between pRIPK3 and pMLKL protein levels, and negative associations of pRIPK3 and pMLKL with gas exchange (DL_{CO}). These data indicate activation of the necroptosis pathway, RIPK3 and the key terminal effector molecule, MLKL, in clinical COPD. Importantly, we observed similar dysregulation of necrosome components in murine experimental COPD, including increased mRNA and protein levels of Mlkl and upstream regulators Ripk1 and Ripk3. Our human and mouse data indicate this dysregulation occurs in multiple cellular compartments including the airways, airway epithelium and pulmonary macrophages. Further delineating the key cellular locations where necroptosis may promote features of COPD will be a future goal.

Having established that necroptosis-related signalling was increased in human and experimental COPD, we tested its role in promoting pathological responses to acute and chronic CS exposure using *Ripk3*$^{-/-}$ and *Mlkl*$^{-/-}$ mice. Deletion of *Ripk3* or *Mlkl* protected against acute and chronic CS-induced cellular and molecular airway inflammation. Reduced recruitment of neutrophils and macrophages to the airways was observed. Notably, molecular markers of inflammation *Cxcl1* (in *Mlkl*$^{-/-}$), *Mmp12*, *Ym1* and *Marco* were suppressed in lung tissue of *Ripk3*$^{-/-}$ and/or *Mlkl*$^{-/-}$ mice in both acute and chronic CS settings. Suppression of other

AJRCCM Articles in Press. Published June 16, 2021 as 10.1164/rccm.202009-3442OC

chemoattractants, such as CXCL2, IFNγ, complement, etc, are likely responsible for the reduced neutrophils in *Ripk3*$^{-/-}$ mice. These molecules are all involved in promoting airway macrophage-related inflammation, and RNA-sequencing analysis of isolated alveolar macrophages from 4-week CS-exposed mice demonstrated increased mRNA expression of all three factors as well as *Mmp12* and *Marco* compared to air-exposed mice. Marco is a scavenger receptor on the surface of macrophages (47). It promotes inflammation by binding and inducing the phagocytosis of low-density lipoprotein and pathogen-associated molecular patterns (48), but is also important for removal of these same ligands. The chitinase like protein YM1 is a marker of alternatively activated macrophages but is also able to induce neutrophil recruitment through expansion of IL-17-producing γδT-cells (49). There have been no studies of YM1 positive macrophages in COPD. The decrease in *Marco* and *Ym1* expression (putative M2 markers) in *Ripk3*$^{-/-}$ and *Mlkl*$^{-/-}$ mice corresponded with reduced macrophage numbers and may represent the suppression of inflammatory activation of these cells or could reflect an overall modulation of macrophage phenotypic subsets in response to CS exposure. Previous studies in COPD patients suggest that M1 and M2 macrophages dominate in the airway wall and lumen, respectively (50). Reductions in CS-induced expression of *Mmp12* were more pronounced with chronic compared to acute CS exposures in both deficient mouse strains. Mmp12 is an enzyme that breaks down extracellular matrix that can be generated through macrophage activation. It is highly upregulated in smokers and associated with the development of emphysema (51), and also contributes to experimental COPD (52). These data suggest that the protective effects of *Ripk3* or *Mlkl* deletion may occur through the suppression of inflammatory activation of macrophages and reduced macrophage production of emphysema-inducing factors. The role of necrosome components in macrophage activation is poorly understood, however, genetic deletion of necroptosis in CS exposure models may alter macrophage activation status indirectly through blockade of pro-inflammatory DAMP release or other responses (53).

AJRCCM Articles in Press. Published June 16, 2021 as 10.1164/rccm.202009-3442OC

Prior studies have linked acute CS exposure to the induction of necroptosis and release of DAMPs that promote airway inflammation. CSE exposure of lung epithelial cells induced MLKL phosphorylation (54). Administration of the RIPK1 kinase inhibitor necrostatin-1 can inhibit CSE-induced death of lung epithelial cells *in vitro*, and reduces DAMP release and neutrophilic airway inflammation during acute CS exposure of mice (54, 55). However, necrostatin-1 has off-target effects and RIPK1 has roles in proinflammatory cytokine signaling and apoptosis. Our data extend these findings by demonstrating roles for core necrosome components RIPK3 and MLKL in CS-induced airway inflammation and show that both airway epithelium and alveolar macrophages are important sites of dysfunction of this pathway. Increased expression of necrosome components could sensitize cells to undergo necroptosis (54, 56-61), and further mechanisms that inhibit necroptosis under physiological circumstances may be suppressed by CS exposure. A recent study demonstrated that the transcript levels of *CFLAR*, an apoptosis and necroptosis modulator, were reduced in lung biopsies of smokers *versus* non-smokers and in epithelial cells following CS exposure *in vitro* (62). *CFLAR* encodes c-FLIP proteins, which heterodimerize with caspase-8 to modulate their cell death-related activities, including suppression of necroptosis (62). Knockdown of *CFLAR* sensitized epithelial cells to CS-induced cell death and related DAMP release, demonstrating a further potential mechanism whereby CS exposure induces necroptosis in the lung. Further studies are required to understand the mechanisms of CS-mediated modulation of signalling upstream of necrosome formation and activation *in vivo*.

Apoptosis has long been considered to have roles in lung remodelling and tissue destruction in COPD, particularly emphysema. Early studies reported increased cell death (TUNEL-positivity) in emphysematous regions of COPD lungs (63), however, TUNEL staining is not a *bona fide* marker of apoptosis and also detect cells undergoing necrosis including necroptosis (62). Furthermore, there is a lack of studies demonstrating the effect or

AJRCCM Articles in Press. Published June 16, 2021 as 10.1164/rccm.202009-3442OC

lack of protection afforded by inhibiting apoptosis (or other types of cell death) in experimental COPD. Thus, the pathogenic roles of apoptosis and broader mechanisms of cell death was unclear. CSE is reported to induce apoptotic cell death of epithelial cells, resulting in TUNEL-positive staining (64). Consistent with this observation, using TUNEL staining, we found that CS exposure significantly increased cell death in the lung parenchyma from 8-weeks onward. Positive cells occurred in the airways, parenchyma and immune cells but were not more prominent in a particular cell type. We attempted unsuccessfully to perform co-staining for TUNEL and active caspase-3. Importantly this increased incidence of cell death was not present at 4 weeks and coincided with the development of emphysema, which is observed from 8 weeks onward in our model (17, 23-30). Thus, the induction of alveolar epithelial cell death may be an important pathophysiological event that contributes to the destruction of alveolar structures in emphysema. Importantly, our data suggest that necroptosis, but not apoptosis, promote destruction of alveoli in CS-induced emphysema. Both genetic deletion of necroptosis-related genes and pharmacological inhibition of apoptosis reduced airway inflammation. Our approach to inhibit apoptosis was to employ a pan-caspase inhibitor. Although this was sufficient to suppress TUNEL-positivity and levels of cleaved caspase-3 in the lungs in experimental COPD, it is likely that pharmacological inhibition was not completely efficient and did not reduce airway remodelling or emphysema. Previous studies showed that these chronic disease features can occur independently of chronic inflammation, such as in the absence of *Ccr5* (65). Moreover, we cannot exclude that some other inflammatory processes not affected by caspase inhibition contributed to the induction of pathological remodelling and emphysema. Also, this approach may have blocked processes additional to apoptosis, such as inflammasome-associated caspase-1 activity and IL-1β production (66). The observation that BALF lymphocytes were increased by dual blockade of apoptosis and necroptosis following CS exposure is intriguing and merits further investigation in terms of the role of cell death in

AJRCCM Articles in Press. Published June 16, 2021 as 10.1164/rccm.202009-3442OC

regulating lymphocyte survival during ongoing inflammatory processes. Additional inhibitory approaches targeting other components of the apoptosis machinery are required to fully delineate the role of apoptosis in pathogenesis of experimental COPD. That apoptosis is usually a non-inflammatory form of cell death while necroptosis is proinflammatory may explain why blocking apoptosis or necroptosis both reduce cell death, but only blocking of necroptosis reduces remodelling and emphysema. However, this does not mean that our finding conflict with previous work indicting that apoptosis contributes to lung remodelling and emphysema. This is because most previous studies used non-specific measurements to evaluate the level of apoptosis which could not separate it from necroptosis. Furthermore, most evidence supporting a role of apoptosis in emphysema is based on clinical studies without causative data.

Our study has some other limitations. Some of the experimental studies would benefit from an increase in sample size. It is currently not possible to confirm activation of the necrosome components through co-immunoprecipitation or detection of phosphorylated necrosome in experimental COPD as there are no specific antibody tools for mice. However, we did detect increased phosphorylation of RIPK3 and MLKL, which reflects necroptosis activation, in human lung resections. In addition, deletion of two separate necrosome components (RIPK3 and MLKL) strongly support roles for necroptosis-related signalling in promoting experimental COPD. This shows that the effects are through necroptosis rather than inflammatory signalling. It is possible that using pharmacological inhibition of caspases may not have completely inhibited apoptosis at all times or in all tissues and cells, however, we confirmed reduction of total lung cell death in pan-caspase-treated CS-exposed mice. The use of caspase-3 specific inhibitors or genetic models of apoptosis inhibition may be useful in future studies to separate apoptotic *versus* non-apoptotic roles of caspases in experimental COPD. Future studies should employ novel inhibitors of necroptosis, which will also be necessary to further establish the therapeutic potential of targeting necroptosis in COPD. Our

AJRCCM Articles in Press. Published June 16, 2021 as 10.1164/rccm.202009-3442OC

study is unique in that we used defined genetic or pharmacological inhibition to specifically delineate the contribution of cell death pathways to experimental COPD pathology; together with measurements of *bona fide* markers of necroptotic cell death in COPD patient lungs. Our study is unique in that we used defined genetic or pharmacological inhibition to specifically delineate the contribution of cell death pathways to experimental COPD pathology; together with measurements of *bona fide* markers of necroptotic cell death in COPD patient lungs.

In summary, we provide compelling evidence that the necroptosis pathway is increased in the lungs in human and experimental COPD. Genetic and pharmacological inhibition shows that RIPK3 and MLKL promote cell death and contribute to the pathogenesis of airway inflammation, remodelling and emphysema. Inhibiting necroptosis may be a novel therapeutic approach in COPD.

Acknowledgements

The authors thank Professors John Silke, Walter and Eliza Hall Institute and Vishva Dixit from Genentech, Inc. for the provision of *Ripk3*$^{-/-}$ mice.

AJRCCM Articles in Press. Published June 16, 2021 as 10.1164/rccm.202009-3442OC

References

1. Vogelmeier CF, Criner GJ, Martinez FJ, Anzueto A, Barnes PJ, Bourbeau J, Celli BR, Chen R, Decramer M, Fabbri LM, Frith P, Halpin DM, Lopez Varela MV, Nishimura M, Roche N, Rodriguez-Roisin R, Sin DD, Singh D, Stockley R, Vestbo J, Wedzicha JA, Agusti A. Global Strategy for the Diagnosis, Management and Prevention of Chronic Obstructive Lung Disease 2017 Report: GOLD Executive Summary. *Respirology* 2017; 22: 575-601.

2. Giordano RJ, Lahdenranta J, Zhen L, Chukwueke U, Petrache I, Langley RR, Fidler IJ, Pasqualini R, Tuder RM, Arap W. Targeted induction of lung endothelial cell apoptosis causes emphysema-like changes in the mouse. *J Biol Chem* 2008; 283: 29447-29460.

3. Tuder RM, Petrache I. Pathogenesis of chronic obstructive pulmonary disease. *J Clin Invest* 2012; 122: 2749-2755.

4. Hou HH, Cheng SL, Liu HT, Yang FZ, Wang HC, Yu CJ. Elastase induced lung epithelial cell apoptosis and emphysema through placenta growth factor. *Cell Death Dis* 2013; 4: e793.

5. Kono H, Rock KL. How dying cells alert the immune system to danger. *Nature reviews Immunology* 2008; 8: 279-289.

6. Samson AL, Zhang Y, Geoghegan ND, Gavin XJ, Davies KA, Mlodzianoski MJ, Whitehead LW, Frank D, Garnish SE, Fitzgibbon C, Hempel A, Young SN, Jacobsen AV, Cawthorne W, Petrie EJ, Faux MC, Shield-Artin K, Lalaoui N, Hildebrand JM, Silke J, Rogers KL, Lessene G, Hawkins ED, Murphy JM. MLKL trafficking and accumulation at the plasma membrane control the kinetics and threshold for

AJRCCM Articles in Press. Published June 16, 2021 as 10.1164/rccm.202009-3442OC

necroptosis. *Nat Commun* 2020; 11: 3151.

7. Kaczmarek A, Vandenabeele P, Krysko DV. Necroptosis: the release of damage-associated molecular patterns and its physiological relevance. *Immunity* 2013; 38: 209-223.

8. Grootjans S, Vanden Berghe T, Vandenabeele P. Initiation and execution mechanisms of necroptosis: an overview. *Cell Death Differ* 2017; 24: 1184-1195.

9. Haw TJ, Starkey MR, Pavlidis S, Fricker M, Arthurs AL, Nair PM, Liu G, Hanish I, Kim RY, Foster PS, Horvat JC, Adcock IM, Hansbro PM. Toll-like receptor 2 and 4 have opposing roles in the pathogenesis of cigarette smoke-induced chronic obstructive pulmonary disease. *American journal of physiology Lung cellular and molecular physiology* 2018; 314: L298-L317.

10. Bezemer GF, Sagar S, van Bergenhenegouwen J, Georgiou NA, Garssen J, Kraneveld AD, Folkerts G. Dual role of Toll-like receptors in asthma and chronic obstructive pulmonary disease. *Pharmacological reviews* 2012; 64: 337-358.

11. Barnes PJ. The cytokine network in chronic obstructive pulmonary disease. *Am J Respir Cell Mol Biol* 2009; 41: 631-638.

12. Pouwels SD, Zijlstra GJ, van der Toorn M, Hesse L, Gras R, Ten Hacken NH, Krysko DV, Vandenabeele P, de Vries M, van Oosterhout AJ, Heijink IH, Nawijn MC. Cigarette smoke-induced necroptosis and DAMP release trigger neutrophilic airway inflammation in mice. *Am J Physiol Lung Cell Mol Physiol* 2016; 310: L377-386.

13. Van Eeckhoutte H, Verhamme F, Lu Z, Buyle-Huybrecht T, Brusselle G, Vandenabeele P, Vandenberghe T, Fricker M, Hansbro P, Bracke K. LSC - 2019 - Role of necroptosis in the pathogenesis of COPD. *Eur Respir J* 2019; 54: 282.

AJRCCM Articles in Press. Published June 16, 2021 as 10.1164/rccm.202009-3442OC

14. Fricker M LZ, Van Eeckhoutte H, Liu G, Verhamme F, Buyle-Huybrecht T, Brusselle G, Murphy J, Bracke K, Hansbro P. Necroptosis is activated in and drives pathogenesis of COPD. *Respirology* 2019; 24 (1): 71.

15. Verhamme F VEH, Buyle-Huybrecht T, Brusselle G, Vandenabeele P, Vanden Berghe T, Bracke K. Expression of receptor interacting protein kinase-3 and mixed lineage kinase domain-like protein in patients with COPD. *Am J Respir Crit Care Med* 2019; 199.

16. Maes T, Bracke KR, Vermaelen KY, Demedts IK, Joos GF, Pauwels RA, Brusselle GG. Murine TLR4 is implicated in cigarette smoke-induced pulmonary inflammation. *Int Arch Allergy Immunol* 2006; 141: 354-368.

17. Beckett EL, Stevens RL, Jarnicki AG, Kim RY, Hanish I, Hansbro NG, Deane A, Keely S, Horvat JC, Yang M, Oliver BG, van Rooijen N, Inman MD, Adachi R, Soberman RJ, Hamadi S, Wark PA, Foster PS, Hansbro PM. A new short-term mouse model of chronic obstructive pulmonary disease identifies a role for mast cell tryptase in pathogenesis. *J Allergy Clin Immunol* 2013; 131: 752-762.

18. Verhamme FM, De Smet EG, Van Hooste W, Delanghe J, Verleden SE, Joos GF, Brusselle GG, Bracke KR. Bone morphogenetic protein 6 (BMP-6) modulates lung function, pulmonary iron levels and cigarette smoke-induced inflammation. *Mucosal Immunol* 2019; 12: 340-351.

19. Dobin A, Davis CA, Schlesinger F, Drenkow J, Zaleski C, Jha S, Batut P, Chaisson M, Gingeras TR. STAR: ultrafast universal RNA-seq aligner. *Bioinformatics* 2013; 29: 15-21.

20. Ritchie ME, Phipson B, Wu D, Hu Y, Law CW, Shi W, Smyth GK. limma powers

AJRCCM Articles in Press. Published June 16, 2021 as 10.1164/rccm.202009-3442OC

differential expression analyses for RNA-sequencing and microarray studies. *Nucleic Acids Res* 2015; 43: e47.

21. Murphy JM, Czabotar PE, Hildebrand JM, Lucet IS, Zhang JG, Alvarez-Diaz S, Lewis R, Lalaoui N, Metcalf D, Webb AI, Young SN, Varghese LN, Tannahill GM, Hatchell EC, Majewski IJ, Okamoto T, Dobson RC, Hilton DJ, Babon JJ, Nicola NA, Strasser A, Silke J, Alexander WS. The pseudokinase MLKL mediates necroptosis via a molecular switch mechanism. *Immunity* 2013; 39: 443-453.

22. Newton K, Sun X, Dixit VM. Kinase RIP3 is dispensable for normal NF-kappa Bs, signaling by the B-cell and T-cell receptors, tumor necrosis factor receptor 1, and Toll-like receptors 2 and 4. *Mol Cell Biol* 2004; 24: 1464-1469.

23. Hansbro PM, Hamilton MJ, Fricker M, Gellatly SL, Jarnicki AG, Zheng D, Frei SM, Wong GW, Hamadi S, Zhou S, Foster PS, Krilis SA, Stevens RL. Importance of mast cell Prss31/transmembrane tryptase/tryptase-gamma in lung function and experimental chronic obstructive pulmonary disease and colitis. *J Biol Chem* 2014; 289: 18214-18227.

24. Fricker M, Deane A, Hansbro PM. Animal models of chronic obstructive pulmonary disease. *Expert opinion on drug discovery* 2014; 9: 629-645.

25. Vlahos R, Bozinovski S. Recent advances in pre-clinical mouse models of COPD. *Clin Sci (Lond)* 2014; 126: 253-265.

26. Hsu AC, Starkey MR, Hanish I, Parsons K, Haw TJ, Howland LJ, Barr I, Mahony JB, Foster PS, Knight DA, Wark PA, Hansbro PM. Targeting PI3K-p110alpha Suppresses Influenza Virus Infection in Chronic Obstructive Pulmonary Disease. *Am J Respir Crit Care Med* 2015; 191: 1012-1023.

AJRCCM Articles in Press. Published June 16, 2021 as 10.1164/rccm.202009-3442OC

27. Tay HL, Kaiko GE, Plank M, Li J, Maltby S, Essilfie AT, Jarnicki A, Yang M, Mattes J, Hansbro PM, Foster PS. Antagonism of miR-328 increases the antimicrobial function of macrophages and neutrophils and rapid clearance of non-typeable Haemophilus influenzae (NTHi) from infected lung. *PLoS Pathog* 2015; 11: e1004549.

28. Thorburn AN, Tseng HY, Donovan C, Hansbro NG, Jarnicki AG, Foster PS, Gibson PG, Hansbro PM. TLR2, TLR4 AND MyD88 Mediate Allergic Airway Disease (AAD) and Streptococcus pneumoniae-Induced Suppression of AAD. *PLoS One* 2016; 11: e0156402.

29. Liu G, Cooley MA, Jarnicki AG, Hsu AC, Nair PM, Haw TJ, Fricker M, Gellatly SL, Kim RY, Inman MD, Tjin G, Wark PA, Walker MM, Horvat JC, Oliver BG, Argraves WS, Knight DA, Burgess JK, Hansbro PM. Fibulin-1 regulates the pathogenesis of tissue remodeling in respiratory diseases. *JCI Insight* 2016; 1.

30. Jarnicki AG, Schilter H, Liu G, Wheeldon K, Essilfie AT, Foot JS, Yow TT, Jarolimek W, Hansbro PM. The inhibitor of semicarbazide-sensitive amine oxidase, PXS-4728A, ameliorates key features of chronic obstructive pulmonary disease in a mouse model. *Br J Pharmacol* 2016; 173: 3161-3175.

31. Conickx G, Mestdagh P, Avila Cobos F, Verhamme FM, Maes T, Vanaudenaerde BM, Seys LJ, Lahousse L, Kim RY, Hsu AC, Wark PA, Hansbro PM, Joos GF, Vandesompele J, Bracke KR, Brusselle GG. MicroRNA Profiling Reveals a Role for MicroRNA-218-5p in the Pathogenesis of Chronic Obstructive Pulmonary Disease. *Am J Respir Crit Care Med* 2017; 195: 43-56.

32. Hsu AC, Dua K, Starkey MR, Haw TJ, Nair PM, Nichol K, Zammit N, Grey ST, Baines KJ, Foster PS, Hansbro PM, Wark PA. MicroRNA-125a and -b inhibit A20 and

AJRCCM Articles in Press. Published June 16, 2021 as 10.1164/rccm.202009-3442OC

MAVS to promote inflammation and impair antiviral response in COPD. *JCI Insight* 2017; 2: e90443.

33. Starkey MR, Plank MW, Casolari P, Papi A, Pavlidis S, Guo Y, Cameron GJM, Haw TJ, Tam A, Obiedat M, Donovan C, Hansbro NG, Nguyen DH, Nair PM, Kim RY, Horvat JC, Kaiko GE, Durum SK, Wark PA, Sin DD, Caramori G, Adcock IM, Foster PS, Hansbro PM. IL-22 and its receptors are increased in human and experimental COPD and contribute to pathogenesis. *Eur Respir J* 2019; 54.

34. D'Hulst A I, Vermaelen KY, Brusselle GG, Joos GF, Pauwels RA. Time course of cigarette smoke-induced pulmonary inflammation in mice. *Eur Respir J* 2005; 26: 204-213.

35. Bracke KR, D'Hulst A I, Maes T, Moerloose KB, Demedts IK, Lebecque S, Joos GF, Brusselle GG. Cigarette smoke-induced pulmonary inflammation and emphysema are attenuated in CCR6-deficient mice. *J Immunol* 2006; 177: 4350-4359.

36. Seys LJ, Verhamme FM, Schinwald A, Hammad H, Cunoosamy DM, Bantsimba-Malanda C, Sabirsh A, McCall E, Flavell L, Herbst R, Provoost S, Lambrecht BN, Joos GF, Brusselle GG, Bracke KR. Role of B Cell-Activating Factor in Chronic Obstructive Pulmonary Disease. *Am J Respir Crit Care Med* 2015; 192: 706-718.

37. Ding J, Lu Q, Ouyang Y, Mao H, Zhang P, Yao J, Xu C, Li X, Xiao J, Zhang Q. A long noncoding RNA regulates photoperiod-sensitive male sterility, an essential component of hybrid rice. *Proc Natl Acad Sci U S A* 2012; 109: 2654-2659.

38. Haw TJ, Starkey MR, Nair PM, Pavlidis S, Liu G, Nguyen DH, Hsu AC, Hanish I, Kim RY, Collison AM, Inman MD, Wark PA, Foster PS, Knight DA, Mattes J, Yagita H, Adcock IM, Horvat JC, Hansbro PM. A pathogenic role for tumor necrosis factor-

AJRCCM Articles in Press. Published June 16, 2021 as 10.1164/rccm.202009-3442OC

related apoptosis-inducing ligand in chronic obstructive pulmonary disease. *Mucosal Immunol* 2016; 9: 859-872.

39. Starkey MR, Nguyen DH, Brown AC, Essilfie AT, Kim RY, Yagita H, Horvat JC, Hansbro PM. Programmed Death Ligand 1 Promotes Early-Life Chlamydia Respiratory Infection-Induced Severe Allergic Airway Disease. *Am J Respir Cell Mol Biol* 2016; 54: 493-503.

40. Fricker M, Goggins BJ, Mateer S, Jones B, Kim RY, Gellatly SL, Jarnicki AG, Powell N, Oliver BG, Radford-Smith G, Talley NJ, Walker MM, Keely S, Hansbro PM. Chronic cigarette smoke exposure induces systemic hypoxia that drives intestinal dysfunction. *JCI Insight* 2018; 3.

41. Horvat JC, Beagley KW, Wade MA, Preston JA, Hansbro NG, Hickey DK, Kaiko GE, Gibson PG, Foster PS, Hansbro PM. Neonatal chlamydial infection induces mixed T-cell responses that drive allergic airway disease. *Am J Respir Crit Care Med* 2007; 176: 556-564.

42. Clauss M, Voswinckel R, Rajashekhar G, Sigua NL, Fehrenbach H, Rush NI, Schweitzer KS, Yildirim AO, Kamocki K, Fisher AJ, Gu Y, Safadi B, Nikam S, Hubbard WC, Tuder RM, Twigg HL, 3rd, Presson RG, Sethi S, Petrache I. Lung endothelial monocyte-activating protein 2 is a mediator of cigarette smoke-induced emphysema in mice. *J Clin Invest* 2011; 121: 2470-2479.

43. Bracke KR, Verhamme FM, Seys LJ, Bantsimba-Malanda C, Cunoosamy DM, Herbst R, Hammad H, Lambrecht BN, Joos GF, Brusselle GG. Role of CXCL13 in cigarette smoke-induced lymphoid follicle formation and chronic obstructive pulmonary disease. *Am J Respir Crit Care Med* 2013; 188: 343-355.

AJRCCM Articles in Press. Published June 16, 2021 as 10.1164/rccm.202009-3442OC

44. De Smet EG, Van Eeckhoutte HP, Avila Cobos F, Blomme E, Verhamme FM, Provoost S, Verleden SE, Venken K, Maes T, Joos GF, Mestdagh P, Brusselle GG, Bracke KR. The role of miR-155 in cigarette smoke-induced pulmonary inflammation and COPD. *Mucosal Immunol* 2020; 13: 423-436.

45. Newton K, Dugger DL, Wickliffe KE, Kapoor N, de Almagro MC, Vucic D, Komuves L, Ferrando RE, French DM, Webster J, Roose-Girma M, Warming S, Dixit VM. Activity of protein kinase RIPK3 determines whether cells die by necroptosis or apoptosis. *Science* 2014; 343: 1357-1360.

46. Wong WW, Vince JE, Lalaoui N, Lawlor KE, Chau D, Bankovacki A, Anderton H, Metcalf D, O'Reilly L, Jost PJ, Murphy JM, Alexander WS, Strasser A, Vaux DL, Silke J. cIAPs and XIAP regulate myelopoiesis through cytokine production in an RIPK1- and RIPK3-dependent manner. *Blood* 2014; 123: 2562-2572.

47. Lara S, Perez-Potti A, Herda LM, Adumeau L, Dawson KA, Yan Y. Differential Recognition of Nanoparticle Protein Corona and Modified Low Density Lipoprotein by Macrophage Receptor with Collagenous Structure. *ACS Nano* 2018.

48. Mukhopadhyay S, Varin A, Chen Y, Liu B, Tryggvason K, Gordon S. SR-A/MARCO-mediated ligand delivery enhances intracellular TLR and NLR function, but ligand scavenging from cell surface limits TLR4 response to pathogens. *Blood* 2011; 117: 1319-1328.

49. Sutherland TE, Logan N, Ruckerl D, Humbles AA, Allan SM, Papayannopoulos V, Stockinger B, Maizels RM, Allen JE. Chitinase-like proteins promote IL-17-mediated neutrophilia in a tradeoff between nematode killing and host damage. *Nat Immunol* 2014; 15: 1116-1125.

AJRCCM Articles in Press. Published June 16, 2021 as 10.1164/rccm.202009-3442OC

50. Eapen MS, Hansbro PM, McAlinden K, Kim RY, Ward C, Hackett TL, Walters EH, Sohal SS. Abnormal M1/M2 macrophage phenotype profiles in the small airway wall and lumen in smokers and chronic obstructive pulmonary disease (COPD). *Sci Rep* 2017; 7: 13392.

51. Woodruff PG, Koth LL, Yang YH, Rodriguez MW, Favoreto S, Dolganov GM, Paquet AC, Erle DJ. A distinctive alveolar macrophage activation state induced by cigarette smoking. *Am J Respir Crit Care Med* 2005; 172: 1383-1392.

52. Hautamaki RD, Kobayashi DK, Senior RM, Shapiro SD. Requirement for macrophage elastase for cigarette smoke-induced emphysema in mice. *Science* 1997; 277: 2002-2004.

53. Choi ME, Price DR, Ryter SW, Choi AMK. Necroptosis: a crucial pathogenic mediator of human disease. *JCI Insight* 2019; 4.

54. Mizumura K, Cloonan SM, Nakahira K, Bhashyam AR, Cervo M, Kitada T, Glass K, Owen CA, Mahmood A, Washko GR, Hashimoto S, Ryter SW, Choi AM. Mitophagy-dependent necroptosis contributes to the pathogenesis of COPD. *J Clin Invest* 2014; 124: 3987-4003.

55. Jie H, He Y, Huang X, Zhou Q, Han Y, Li X, Bai Y, Sun E. Necrostatin-1 enhances the resolution of inflammation by specifically inducing neutrophil apoptosis. *Oncotarget* 2016; 7: 19367-19381.

56. Thapa RJ, Nogusa S, Chen P, Maki JL, Lerro A, Andrake M, Rall GF, Degterev A, Balachandran S. Interferon-induced RIP1/RIP3-mediated necrosis requires PKR and is licensed by FADD and caspases. *Proc Natl Acad Sci U S A* 2013; 110: E3109-3118.

AJRCCM Articles in Press. Published June 16, 2021 as 10.1164/rccm.202009-3442OC

57. Cook WD, Moujalled DM, Ralph TJ, Lock P, Young SN, Murphy JM, Vaux DL. RIPK1- and RIPK3-induced cell death mode is determined by target availability. *Cell Death Differ* 2014; 21: 1600-1612.

58. Sosna J, Voigt S, Mathieu S, Lange A, Thon L, Davarnia P, Herdegen T, Linkermann A, Rittger A, Chan FK, Kabelitz D, Schutze S, Adam D. TNF-induced necroptosis and PARP-1-mediated necrosis represent distinct routes to programmed necrotic cell death. *Cell Mol Life Sci* 2014; 71: 331-348.

59. Nogusa S, Thapa RJ, Dillon CP, Liedmann S, Oguin TH, 3rd, Ingram JP, Rodriguez DA, Kosoff R, Sharma S, Sturm O, Verbist K, Gough PJ, Bertin J, Hartmann BM, Sealfon SC, Kaiser WJ, Mocarski ES, Lopez CB, Thomas PG, Oberst A, Green DR, Balachandran S. RIPK3 Activates Parallel Pathways of MLKL-Driven Necroptosis and FADD-Mediated Apoptosis to Protect against Influenza A Virus. *Cell Host Microbe* 2016; 20: 13-24.

60. Schock SN, Chandra NV, Sun Y, Irie T, Kitagawa Y, Gotoh B, Coscoy L, Winoto A. Induction of necroptotic cell death by viral activation of the RIG-I or STING pathway. *Cell Death Differ* 2017; 24: 615-625.

61. Wang Y, Zhou JS, Xu XC, Li ZY, Chen HP, Ying SM, Li W, Shen HH, Chen ZH. Endoplasmic reticulum chaperone GRP78 mediates cigarette smoke-induced necroptosis and injury in bronchial epithelium. *International journal of chronic obstructive pulmonary disease* 2018; 13: 571-581.

62. Faiz A, Heijink IH, Vermeulen CJ, Guryev V, van den Berge M, Nawijn MC, Pouwels SD. Cigarette smoke exposure decreases CFLAR expression in the bronchial epithelium, augmenting susceptibility for lung epithelial cell death and DAMP

AJRCCM Articles in Press. Published June 16, 2021 as 10.1164/rccm.202009-3442OC

release. *Sci Rep* 2018; 8: 12426.

63. Imai K, Mercer BA, Schulman LL, Sonett JR, D'Armiento JM. Correlation of lung surface area to apoptosis and proliferation in human emphysema. *Eur Respir J* 2005; 25: 250-258.

64. Yamada K, Asai K, Nagayasu F, Sato K, Ijiri N, Yoshii N, Imahashi Y, Watanabe T, Tochino Y, Kanazawa H, Hirata K. Impaired nuclear factor erythroid 2-related factor 2 expression increases apoptosis of airway epithelial cells in patients with chronic obstructive pulmonary disease due to cigarette smoking. *BMC pulmonary medicine* 2016; 16: 27.

65. Bracke KR, D'Hulst A I, Maes T, Demedts IK, Moerloose KB, Kuziel WA, Joos GF, Brusselle GG. Cigarette smoke-induced pulmonary inflammation, but not airway remodelling, is attenuated in chemokine receptor 5-deficient mice. *Clin Exp Allergy* 2007; 37: 1467-1479.

66. Pinkerton JW, Kim RY, Robertson AAB, Hirota JA, Wood LG, Knight DA, Cooper MA, O'Neill LAJ, Horvat JC, Hansbro PM. Inflammasomes in the lung. *Mol Immunol* 2017; 86: 44-55.

AJRCCM Articles in Press. Published June 16, 2021 as 10.1164/rccm.202009-3442OC

Figure legends

Figure 1. Protein levels and activation of RIPK3 and MLKL are increased in human COPD lung resections. (*A-D*) Immunohistochemistry for MLKL in clinical samples. (*A*) Representative images of immunohistochemical staining for MLKL in lung tissue sections from never smokers, smokers without airflow limitation, and patients with COPD GOLD II and III-IV. (*B*) Quantification of MLKL positive staining in airway epithelium, n=8-16 (Pbm=perimeter of the basement membrane). (*C*) Micrographs of alveolar macrophages stained for MLKL. (*D*) Semi-quantitative assessment of the MLKL signal in macrophages from never smokers, non-COPD smokers and COPD GOLD II and III-IV, n=8-16. (*E*) Immunoblot of pRIPK3 of lung tissue homogenates from never smokers, smokers without airflow limitation, and patients with COPD GOLD II and III-IV. (*F*) Quantification of pRIPK3 immunoblotting of human lung tissue homogenates, assessed by densitometry, band intensities were normalized to GAPDH, n=10/group. (*G*) Immunoblot of pMLKL on lung tissue homogenates from never smokers, smokers without airflow limitation, and patients with COPD GOLD II and III-IV, n=10/group. (*H*) Quantification of pMLKL immunoblotting of human lung tissue homogenates, assessed by densitometry, band intensities were normalized to GAPDH, n=10/group. (*I*) Spearman correlation between pRIPK3 and pMLKL protein levels. (*J*, *K*) Spearman correlation of pRIPK3 and pMLKL protein levels with DL_{CO} (%). Statistical analyses used the Shapiro-Wilk test to test for normality, then one-way ANOVA with Bonferroni *post-hoc* for multiple comparisons (*D*) or Kruskal-Wallis test with Dunn's multiple comparisons (*B*, *F*, *H*). Spearman rank correlation was used to test for correlations (*I-K*). Results are median±IQR. * compared to other groups indicated. * = P<0.05, ** = P<0.01, *** = P<0.001. GAPDH: glyceraldehyde-3-phosphate dehydrogenase.

Figure 2. Necroptosis-related mRNA and protein levels are increased in the lung in

AJRCCM Articles in Press. Published June 16, 2021 as 10.1164/rccm.202009-3442OC

experimental COPD. (*A*) TUNEL staining in the lungs of normal air- and nose-only cigarette smoke (CS)-exposed mice (4-, 8- and 12-weeks of nose-only CS exposure)， n=3-4/group. *Mlkl* mRNA expression in whole lung tissues relative to *Hprt* housekeeping control after (*B*) 4-, (*C*) 8- and (*D*) 12-weeks, n=6/group. (*E*) Expression of *Mlkl* mRNA after 8 weeks of CS exposure in airway and parenchymal tissue, n=6/group. (*F*) *Ripk1*, (*G*) *Ripk3* and (*H*) *Mlkl* mRNA expression in alveolar macrophages sorted by flow cytometry from BALF of mice exposed to whole body CS for 4 weeks, n=5/group. (*I)* Immunoblot images for Ripk1, Ripk3 and β-actin loading control in whole lung homogenates following 8 weeks of nose-only CS exposure, approximate molecular weights indicated. (*J*) *Ripk1* and (*K*) *Ripk3* changes determined by densitometry normalized to β-actin, n=3/group. (*L*) Immunoblot images for Mlkl and vinculin loading control, approximate molecular weights indicated. (*M*) Mlkl levels determined by densitometry normalized to vinculin, n=5/group. (*N*) Representative images of immunofluorescence staining for MLKL, in airway epithelium and macrophages after 8 weeks of CS exposure. Data are mean ± SEM. * compared to other groups indicated. * = P<0.05, *** = P<0.001. # compared to wild-type air-exposed controls. # = P<0.05, ## = P<0.01, ### = P<0.001, #### = P<0.0001. For data with four groups, one-way ANOVA with Bonferroni correction for multiple comparisons, and for data with two groups, Student's *t-test* was used.

Figure 3. Ripk3 and Mlkl drive airway inflammation in response to acute CS-exposure (1-week exposure, nose-only). Numbers of (*A*) total leukocytes, (*B*) macrophages, (*C*) neutrophils and (*D*) lymphocytes in the BALF in normal air- and cigarette smoke (CS)-exposed wild-type (WT) and *Ripk3*-deficient ($^{-/-}$) mice, n=6/group. Numbers of (*E*) total leukocytes, (*F*) macrophages, (*G*) neutrophils and (*H*) lymphocytes in air- and CS-exposed WT *and Mlkl*$^{-/-}$ mice， n=6/group. Data are mean ± SEM . * compared to other groups indicated. * = P<0.05, **** = P<0.0001. # compared to wild-type air-exposed controls. # = P<0.05, ## = P<0.01, ### = P<0.001, #### = P<0.0001. One-way ANOVA with Bonferroni correction for multiple

AJRCCM Articles in Press. Published June 16, 2021 as 10.1164/rccm.202009-3442OC

comparisons was used.

Figure 4. *Ripk3* deficiency reduces airway inflammation, remodelling and emphysema in experimental COPD (8-week exposure, nose-only). Numbers of (*A*) total leukocytes, (*B*) macrophages, (*C*) neutrophils and (*D*) lymphocytes in the BALF of normal air- and cigarette smoke-exposed wild-type (WT) and *Ripk3*-deficient ($^{-/-}$) mice，n=5-6/group. (*E*) Airway and (*F*) vascular inflammatory score, and (*G*) average macrophage numbers in 15 random fields in lung histology，n=5-6/group. (*H*) Lung sections stained with Sirius red, scale bar = 60 μm. (*I*) collagen deposition and (*J*) epithelial thickness n=4-6/group. (*K*) Lung sections stained with H&E stain, scale bar = 60 μm. and (*L*) mean linear intercept. Data are mean ± SEM. * compared to other groups indicated. * = P<0.05, ** = P<0.01, *** = P<0.01. # compared to WT air-exposed controls. # = P<0.05, ## = P<0.01, ### = P<0.001, #### = P<0.0001. One-way ANOVA with Bonferroni correction for multiple comparisons was used.

Figure 5. *Mlkl* deficiency or caspase inhibition by qVD-OPh treatment reduce chronic CS-induced airway inflammation (8-week exposure, nose-only). Numbers of (*A*) total leukocytes, (*B*) macrophages, (*C*) neutrophils and (*D*) lymphocytes in the BALF of normal air- and cigarette smoke-exposed untreated or qVD-OPh treated wild-type (WT) or *Mlkl*$^{-/-}$ mice n=5-6/group. Mice were treated with qVD-OPh or vehicle 3x/week throughout CS-exposure period. Data are mean ± SEM. * compared to other groups indicated. ** = P<0.01, *** = P<0.001, **** = P<0.0001. # compared to WT air-exposed controls. # = P<0.05, ### = P<0.001, #### = P<0.0001. One-way ANOVA with Bonferroni correction for multiple comparisons was used.

Figure 6. *Mlkl* deficiency or caspase inhibition by qVD-OPh treatment reduce chronic cigarette smoke (CS)-induced lung inflammation, but only *Mlkl* deficiency reduces airway remodelling and emphysema (8-week exposure, nose-only). Lung sections stained with (*A*) Sirius red or (*B*) H&E, scale bar = 60 μm. (*C*) Airway and (*D*) vascular histopathology score, (*E*) average

AJRCCM Articles in Press. Published June 16, 2021 as 10.1164/rccm.202009-3442OC

macrophage numbers in 15 random fields, (*F*) collagen deposition, (*G*) airway epithelial thickness, and (*H*) mean linear intercept in 15 random fields in lung histology of normal air- and CS-exposed untreated or qVD-OPh treated wild-type (WT) or *Mlkl* deficient mice, n=6/group. Mice were treated with qVD-OPh or vehicle 3x/week throughout CS-exposure period. Data are mean ± SEM. * compared to other groups indicated. * = P<0.05, ** = P<0.01, **** = P<0.0001. # compared to wild-type air-exposed controls. ## = P<0.01, ### = P<0.001, #### = P<0.0001. One-way ANOVA with Bonferroni correction for multiple comparisons was used.

Figure 7. *Ripk3* and *Mlkl* deficiency suppresses cell death and caspase-3 activation (8-week exposure, nose-only). (*A*) TUNEL-positive and (*B*) active (cleaved) caspase-3 positive cells in the lungs of normal air- and cigarette smoke (CS)-exposed wild-type (WT) or *Ripk3* deficient ($^{-/-}$) mice, n=5-6/group. (*C*) TUNEL-positive and (*D*) active caspase-3 positive cells in the lungs of normal air- and CS-exposed untreated or qVD-OPh treated WT or *Mlkl*$^{-/-}$ mice, n=6/group. Results are mean ± SEM. * compared to other groups indicated. * = P < 0.05. # compared to WT air-exposed controls. # = P<0.05, ## = P<0.01, ### = P<0.001, #### = P<0.0001. One-way ANOVA with Bonferroni correction for multiple comparisons was used.

AJRCCM Articles in Press. Published June 16, 2021 as 10.1164/rccm.202009-3442OC

Figures

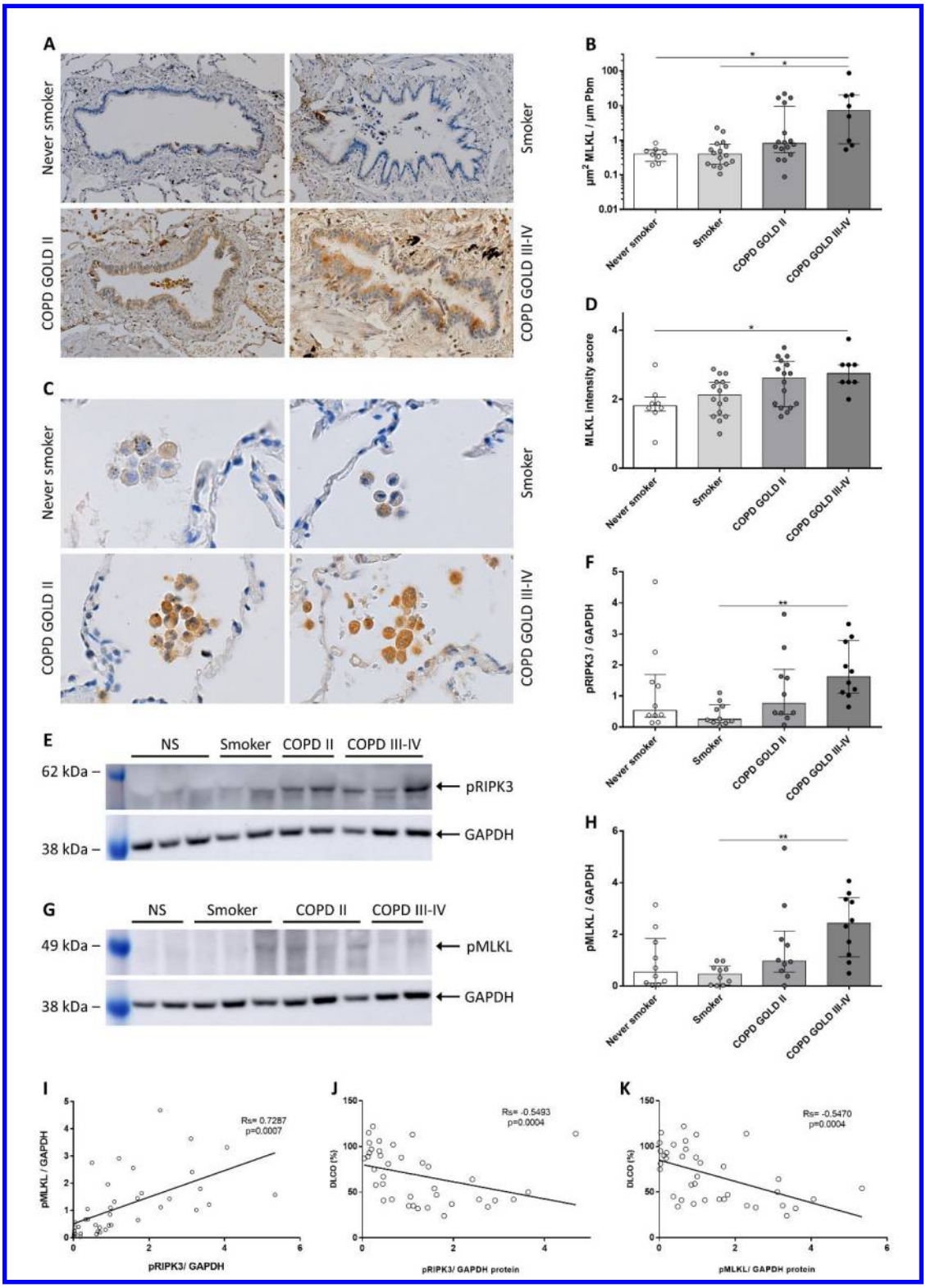

Figure 1

AJRCCM Articles in Press. Published June 16, 2021 as 10.1164/rccm.202009-3442OC

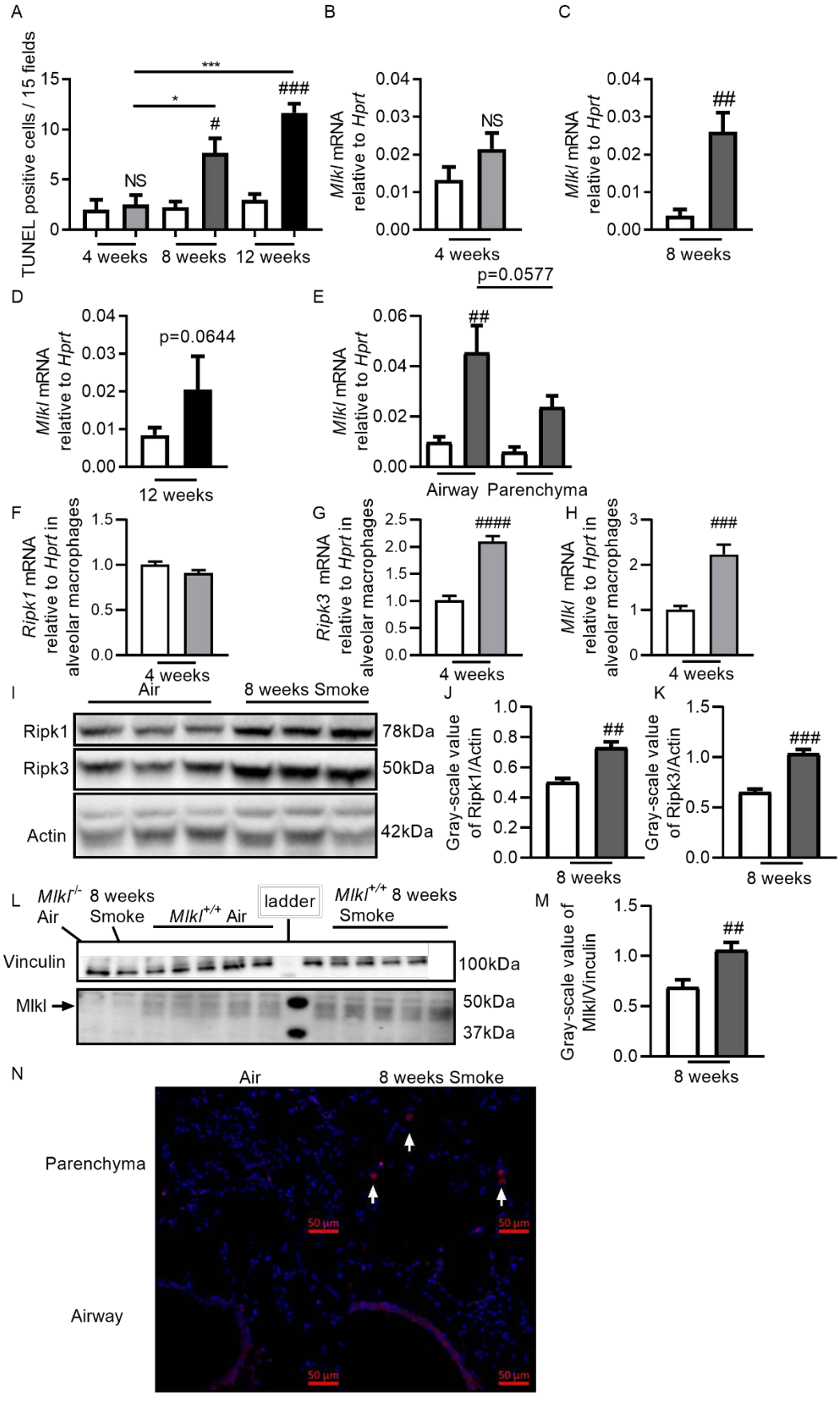

Figure 2

AJRCCM Articles in Press. Published June 16, 2021 as 10.1164/rccm.202009-3442OC

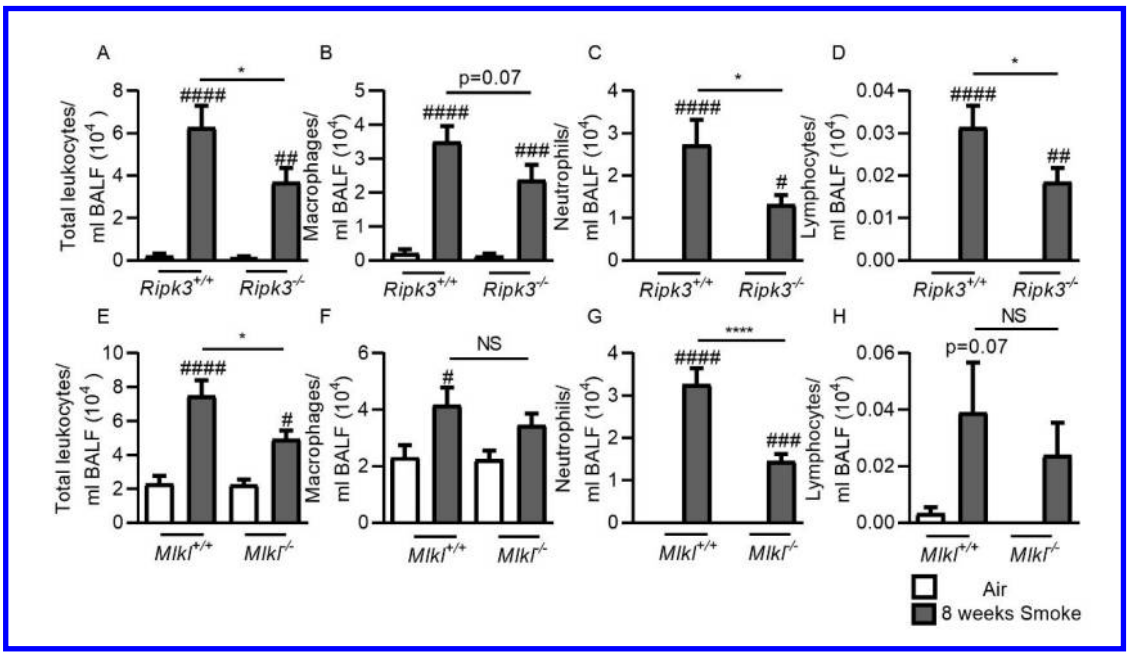

Figure 3

AJRCCM Articles in Press. Published June 16, 2021 as 10.1164/rccm.202009-3442OC

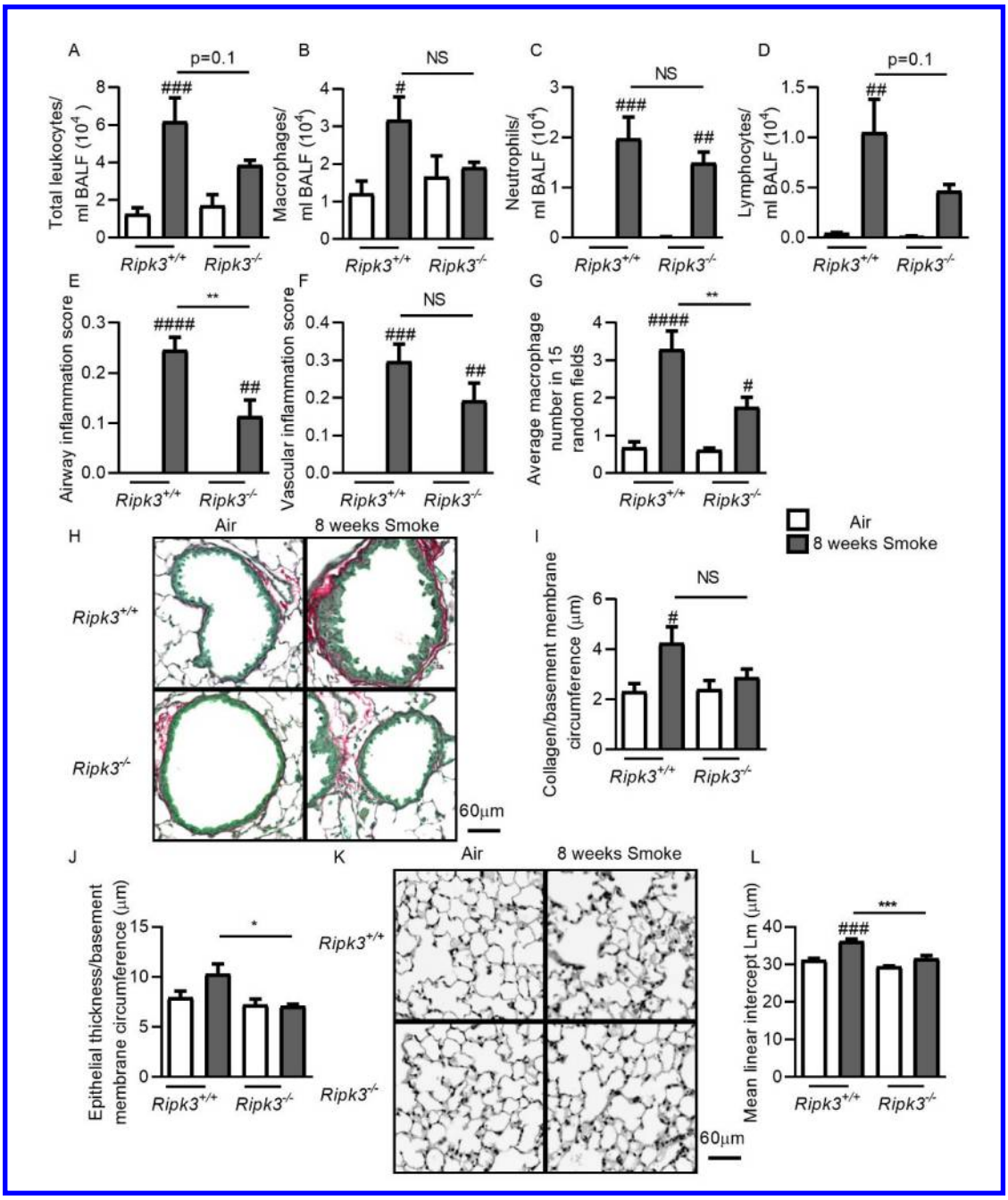

Figure 4

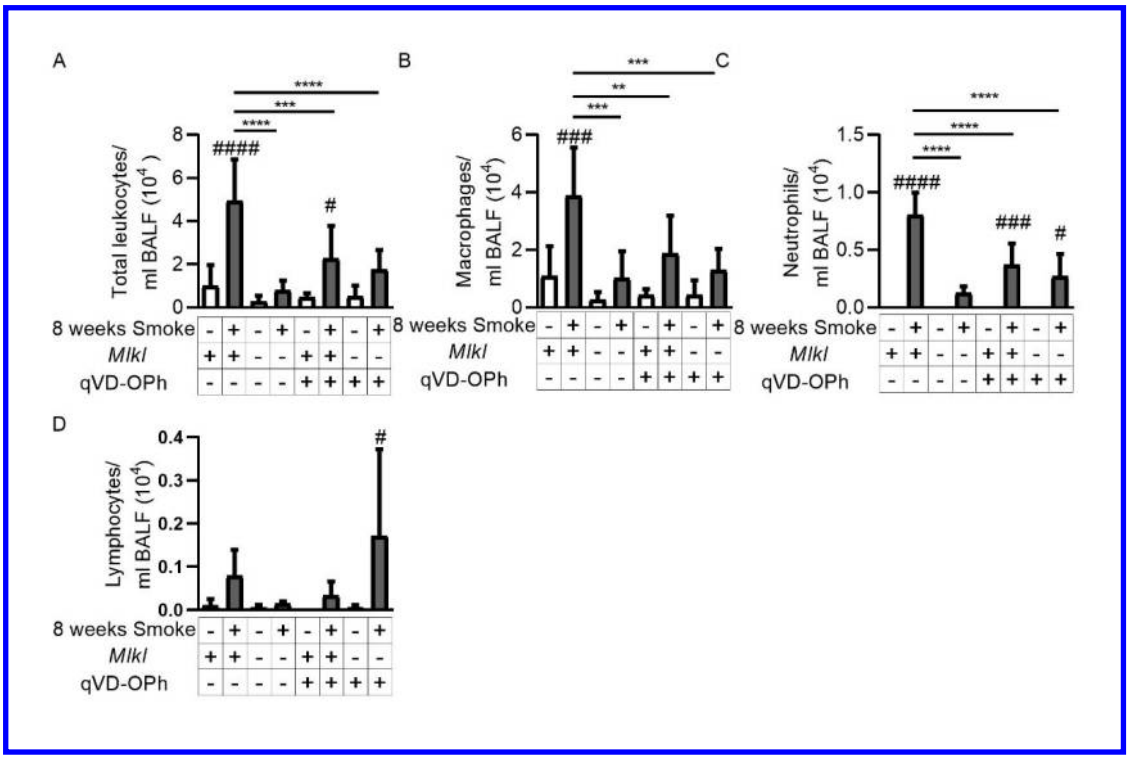

Figure 5

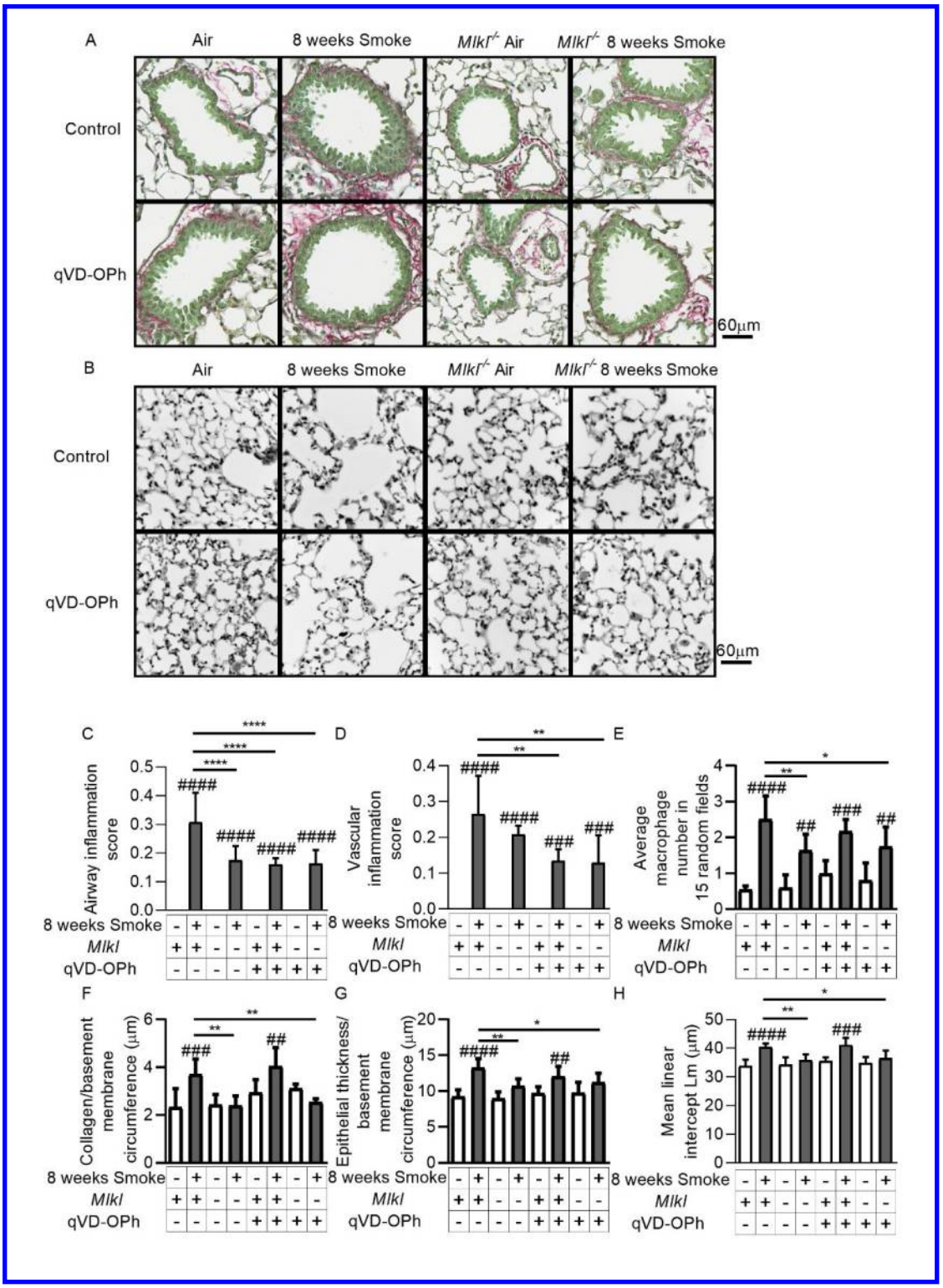

Figure 6

AJRCCM Articles in Press. Published June 16, 2021 as 10.1164/rccm.202009-3442OC

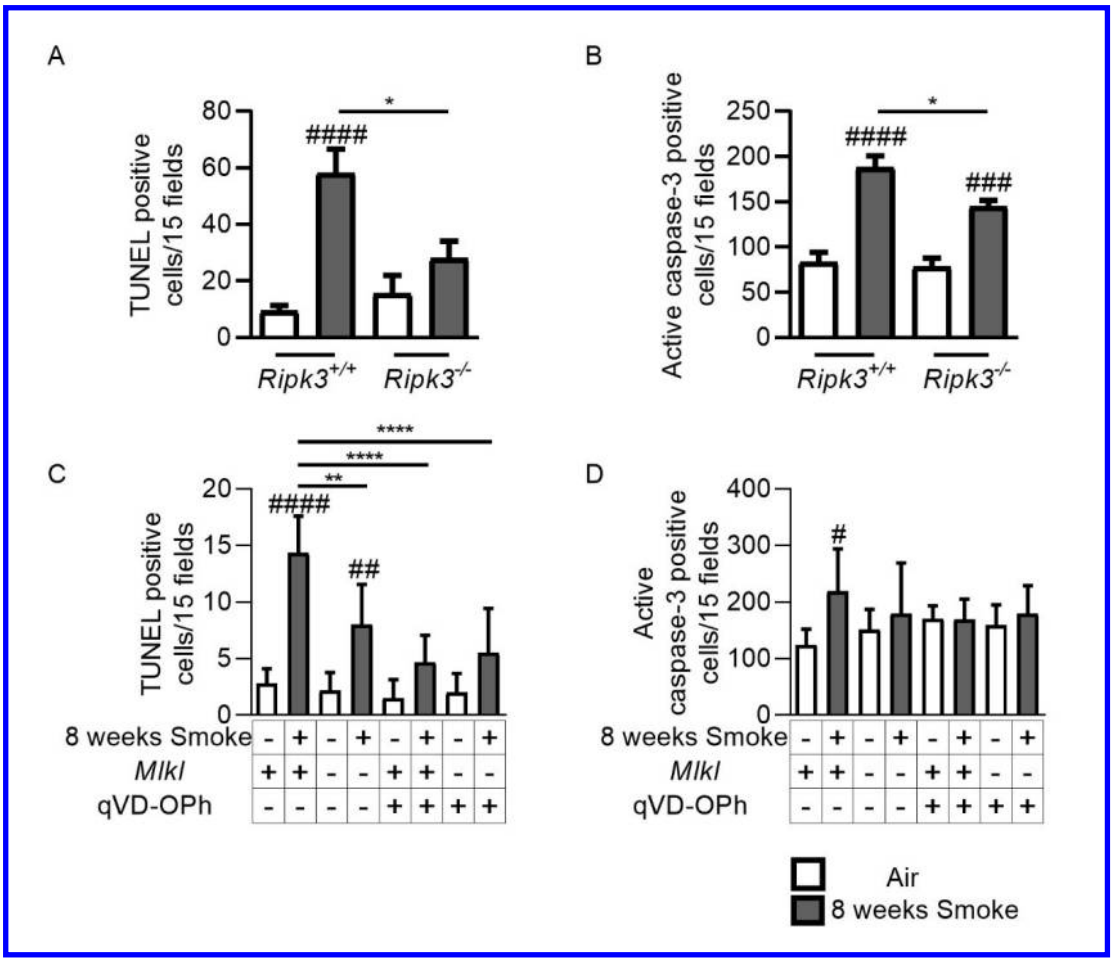

Figure 7

AJRCCM Articles in Press. Published June 16, 2021 as 10.1164/rccm.202009-3442OC

Necroptosis Signalling Promotes Inflammation, Airway Remodelling and Emphysema in COPD

Zhe Lu[1*], Hannelore P. Van Eeckhoutte[2*], Gang Liu[1,3], Prema M Nair[1], Bernadette Jones[1], Caitlin M. Gillis[3,4,5], B. Christina Nalkurthi[3], Fien Verhamme[2], Tamariche Buyle-Huybrecht[2], Peter Vandenabeele[4,5], Tom Vanden Berghe[4,5,6], Guy G. Brusselle[2], James M. Murphy[7], Peter A. Wark[1], Ken R. Bracke[2*], Michael Fricker[1*], Philip M. Hansbro[1,3*]

[1]Priority Research Centre for Healthy Lungs, Hunter Medical Research Institute, University of Newcastle, Newcastle, New South Wales, Australia; [2]Department of Respiratory Medicine, Laboratory for Translational Research in Obstructive Pulmonary Diseases, Ghent University Hospital, Ghent, Belgium; [3]Centre for Inflammation, Centenary Institute and University of Technology Sydney, Faculty of Science, Sydney, New South Wales, Australia; [4]VIB Center for Inflammation Research, Department for Biomedical Molecular Biology, Ghent University, Ghent, Belgium; [5]Methusalem program CEDAR-IC, Ghent University, B-9052 Ghent, Belgium; [6]Department Biomedical Sciences, University of Antwerp, Antwerp, Belgium; [7]Walter and Eliza Hall Institute of Medical Research and Department of Medical Biology, University of Melbourne, Victoria, Australia.

*These authors contributed equally to this manuscript.

Correspondence and requests for reprints should be addressed to Philip M. Hansbro, Ph.D., Centre for Inflammation, Centenary Institute and University of Technology Sydney, School of Life Sciences, Faculty of Science, Sydney, New South Wales 2050, Australia. E-mail: philip.hansbro@uts.edu.au.

AJRCCM Articles in Press. Published June 16, 2021 as 10.1164/rccm.202009-3442OC

Human study population

For immunohistochemistry analyses, lung resection specimens were obtained from 48 patients, of which 40 were from surgery for solitary pulmonary tumors (Ghent University Hospital, Ghent, Belgium) and 8 were from excised lungs from end-stage COPD patients undergoing lung transplantation (University Hospital Gasthuisberg, Leuven, Belgium). The cohort of 48 patients was divided into 4 subgroups: 8 never smokers, 16 smokers without airflow limitation, 16 patients with COPD GOLD stage II, and 8 patients with COPD GOLD stage III-IV (Table E1).

For immunoblot analyses, lung resection specimens were obtained from 40 patients, of which 30 were from surgery for solitary pulmonary tumours (Ghent University Hospital, Ghent, Belgium) and 10 were from excised lungs from end-stage COPD patients undergoing lung transplantation (University Hospital Gasthuisberg, Leuven, Belgium). The cohort of 40 patients was divided into 4 subgroups: 10 never smokers, 10 smokers without airflow limitation, 10 patients with COPD GOLD stage II and 10 patients with COPD GOLD stage III-IV (Table E2).

Lung tissue from resected specimens was harvested by a pathologist at maximum distance from the tumor. All patients with COPD had stable disease as patients with exacerbations in the previous 2 months were excluded. Other exclusion criteria were chemotherapy or radiotherapy in the previous 6 months, diagnosis of mesothelioma or asthma, and infection of the upper or lower respiratory tract in the preceding 4 weeks.

Immunohistochemistry for human MLKL

Paraffin-embedded lung tissues were cut to a thickness of 3µm and placed on poly-L-lysine coated slides (Sigma, St Louis, MO, USA). Sections were deparaffinized with xylene and

AJRCCM Articles in Press. Published June 16, 2021 as 10.1164/rccm.202009-3442OC

rehydrated with ethanol. Subsequently, antigen retrieval was performed using an EDTA buffer (Dako, Glostrup, Denmark). After blocking of endogenous peroxidase activity with 3% hydrogen peroxide (Merck, Darmstadt, Germany) sections were incubated with a streptavidin block (15 min, Vector Laboratories), and a biotin block (15 min, Vector Laboratories). After application of Blocking Reagent (Roche Diagnostics, Mannheim, Germany) with 0.3% Triton, sections were incubated (4°C, overnight) with primary antibody anti-MLKL (1 µg/ml, Merck, rat IgG Cat#MABC604). Control sections were incubated with an isotype mix of rat IgG2a (0.5 µg/ml, BD, Cat#559073, Franklin Lakes, New Jersey, United States) and rat IgG1 (0.5 µg/ml, BD, Cat#559072). Afterwards, secondary antibody biotin-conjugated goat anti-rat (5 µg/ml, BD, Cat#559286) was added, followed by HRP-conjugated streptavidin (Vectastin) and diaminobenzidine substrate (Dako). Finally, sections were counterstained with Mayer's Hematoxylin (Sigma, St. Louis, Missouri, United States), dehydrated with ethanol and xylene and mounted with pertex (Thermo Fisher Scientific, Waltham, MA, USA).

Quantification of human MLKL immunohistochemistry

Quantitative scoring of MLKL-positive area in the airway epithelium was performed in a blinded fashion using AxioVision software (Zeiss, Oberkochen, Germany) (1), (2). Epithelial cells were marked between two lines, one lining the airway lumen the other the basement membrane. The amount of MLKL positive signal in the epithelium was normalized to the perimeter of the basement membrane (Pbm). The final score for each patient was the average MLKL staining in all airways present in all tissue blocks available for that patient. Semi-quantitative scoring of MLKL intensity in macrophages was performed in a blinded fashion by 2 independent observers on 4 lung tissue sections from each subject. The degree of expression in macrophages was defined by a score between 0 and 4 (0: no MLKL staining; 1: very faint MLKL staining intensity; 2: intermediate MLKL staining intensity; 3: strong MLKL staining

AJRCCM Articles in Press. Published June 16, 2021 as 10.1164/rccm.202009-3442OC

intensity; 4: very strong MLKL staining intensity).

Human lung homogenates

To prepare human lung homogenates, tissue blocks from resected samples were snap-frozen in liquid nitrogen and stored at -80°C. Samples were transferred to 1 ml RIPA buffer (Cell Signaling Technology, Danvers, MA, USA) containing Halt™ Protease Inhibitor Cocktail Kit (Thermo Scientific) and 1 PhosStop tablet (Roche) per 10ml lysis buffer. Samples were homogenized on ice using a TissueRuptor (Qiagen, Hilden, Germany), sonicated (4 times for 5 seconds) and then centrifuged (300x*g*, 10 min, 4°C) after which the middle layer was collected. Total protein concentrations were measured using Pierce™ BCA Protein Assay Kits (Thermo Fisher Scientific).

SDS-PAGE and immunoblot of human samples

Lung homogenates (30 µg) were loaded into 10% NuPAGE Bis-Tris Protein Gels and SDS-page electrophoresis was performed using a Mini Gel Tank (Thermo Fisher Scientific) (3). Proteins were transferred to Novex® PVDF membranes (Thermo Fisher Scientific), which was blocked with 5 % milk powder (except for RIPK3 when 5% BSA was used) in TBS-T (120 mM NaCl, 10 mM Tris, pH 8.0) and incubated overnight with the primary antibodies: anti-RIPK3 (1/1,500, Santa Cruz, sc374639), anti-pRIPK3 (1/1,000, Abcam, Cat#Ab209384), anti-MLKL (1/1,000, Abcam, Cat#Ab184718) and anti-pMLKL (1/1,000, Abcam, Cat#Ab187091, Cambridge, United Kingdom). Membranes were then incubated with secondary HRP-conjugated antibody (1/25,000, 1 hour, GE Healthcare) and bands were visualized using SuperSignal™ West Dura Extended Duration Substrate (Thermo Fisher Scientific) or Western Lightning Plus-ECL (Perkin Elmer). GAPDH expression was visualized using HRP-conjugated anti-GAPDH (1/1000, Cell Signaling, Cat#3683). Chemiluminescence images were acquired using the Amersham Imager 600 (GE Healthcare). Immunoblot analysis was

AJRCCM Articles in Press. Published June 16, 2021 as 10.1164/rccm.202009-3442OC

performed using Image J for densitometric quantification using the 'Analyze>Gels' function. Band intensity was measured relative to the band intensity of one lane and normalized to GAPDH expression.

Mice

All mice were generated and maintained in specific pathogen-free conditions. *Mlkl* deficient $^{(-/-)}$ mice (4) were used. *Ripk3*$^{-/-}$ mice (5) were kindly provided by Professor John Silke from the Walter and Eliza Hall Institute of Medical Research, Australia and Dr Vishva Dixit from Genentech, Inc. The *Ripk3*$^{-/-}$ strain was backcrossed on to C57BL/6 background for a minimum of 10 generations, as described (6). *Mlkl*$^{-/-}$ mice were generated on the C57BL/6 background, and *Ripk3*$^{-/-}$ mice were generated on a 129 and C57BL/6N chimeric background and then backcrossed onto the C57BL/6 background. Wild-type (WT) C57BL/6 counterparts were used as controls. All experiments carried out at the University of Newcastle and Ghent are performed with 6-8 week-old female and male mice, respectively. All use of animals met the requirements of the NSW Animal Research Act 1985, NSW Animal Research Regulation 2010 and the Australian code of practice for the care and use of animals for scientific purposes.

Experimental COPD

For each group, 6 mice (Hunter Medical Research Institute) were exposed to mainstream cigarette smoke (CS) from 3R4F cigarettes (University of Kentucky, Lexington, KY, USA) *via* the nose-only in a custom-designed and purpose-built nose-only smoke system (CH Technologies, Westwood, NJ, USA). They were exposed to the smoke of 12 cigarettes per run, 2 runs per day, 5 days per week for up to 12 weeks (chronic exposure) as described extensively previously (7-18). Other mice (Ghent University) were exposed to whole body CS, as described previously (2, 19-21). Briefly, mice (n = 8–9 mice/group) were exposed to the smoke of five 3R4F cigarettes without filters four times a day with 30 min smoke-free intervals, 5 days a

AJRCCM Articles in Press. Published June 16, 2021 as 10.1164/rccm.202009-3442OC

week, for 4 weeks (sub-chronic exposure). All control mice were exposed to normal air.

qVD-OPh intervention

WT and *Mlkl*$^{-/-}$ mice exposed to nose-only CS for 8 weeks were treated with qVD-OPh (Sapphire Bioscience, A14915) intranasally (25 μg, 50 μL volume) as previously published (22), or vehicle (50 μL, 0.25% DMSO in PBS) 3 times per week (Mon, Wed, Fri), prior to the commencement of CS exposure on any given day.

Bronchoalveolar lavage fluid (BALF) and lung tissues

To collect BALF and lungs were collected (7, 14, 15, 23, 24). The chest cavity was opened, the diaphragm punctured and the rib cage carefully cut away to expose the lungs and trachea. An incision was made in the trachea and a blunt end needle (19 G) inserted. The multilobe right lung was tied off. The large left lung lobe was lavaged with two washes of saline (400 μL) administered *via* the trachea and cytospins prepared. Differential cell counts of macrophages, neutrophils, eosinophils and lymphocytes was performed on 200 cells per slide according to morphology (7, 25). The right lung cranial, middle and caudal and post-caval lobes were carefully cut off and each lobe placed in a separate tube and snap frozen in liquid nitrogen. The left lung was perfused *via* the heart with saline to remove excess blood. The lung was then inflated with 10% formalin (500 μL), tied off at the trachea and immersed in 10 % formalin (24 hours, room temperature) for fixation. Formalin was replaced with 70 % ethanol for long-term storage of formalin-fixed tissue.

TUNEL assay

A DeadEnd™ Fluorometric TUNEL System (Promega, Madison, Wisconsin, United States) was used to perform TUNEL assays according to the manufacturer's instructions, which detect the DNA fragments of apoptotic or necrotic-like cell death (26). Briefly, slices of whole lung

AJRCCM Articles in Press. Published June 16, 2021 as 10.1164/rccm.202009-3442OC

histology samples embedded in paraffin were assessed. Paraffin was removed by immersing in xylene (2 x 5 minutes). Residual xylene was washed away by immersing in ethanol (100 %, 5 minutes). Then samples were rehydrated by sequential immersion in four ethanol concentrations (100, 90, 80 and 60%, 3 minutes each). After immersion in 0.85 % NaCl (5 minutes) and Phosphate Buffered Saline (5 minutes, PBS), samples were immersed in 4 % paraformaldehyde (15 minutes), followed by two washes in PBS (5 minutes), and removal off excess liquid. Subsequently the tissue was incubated in proteinase K solution (200 µL, 20 µg/mL, 9 minutes, room temperature). Samples were then sequentially immersed in PBS (5 minutes), 4 % paraformaldehyde (5 minutes) and PBS (5 minutes). Tissue was then covered with equilibration buffer at (100 µL, room temperature, 10 minutes), and the enzymatic TUNEL reaction performed in 45 µL equilibration buffer, 5 µL nucleotide mix and 1 µL Terminal Deoxynucleotidyl Transferase, Recombinant (rTdT) enzyme for each sample. Each was covered with a plastic coverslip and incubated in a humidified chamber (in the dark, 60 minutes, 37 ^{0}C). Two Saline Sodium Citrate (SSC) immersions (15 minutes) terminated the TUNEL reaction. Samples were then washed in PBS and immersed in Hoechst 33342 (5 µg/mL, 5 minutes, Sigma-Aldrich). Samples were further washed with PBS, excess liquid removed, and coverslips mounted with Fluoromount (Merck Millipore). For each sample, 15 random views (with only lung parenchyma, without the edge of the lung, airways or blood vessels) were generated using a 40X objective with a light microscope (BX41, Olympus, Japan) and ImagePro Plus software (version 7). The number of positive signals per field was quantified.

Immunofluorescence staining for mouse MLKL

Lungs of mice exposed to nose-only CS or normal air for 8 weeks 8 and OCT inflated were cryosectioned at 8µm and fixed in 100% methanol for 30 minutes. Tissues were then washed

AJRCCM Articles in Press. Published June 16, 2021 as 10.1164/rccm.202009-3442OC

with Dulbecco's Phosphate Buffered Saline and blocked in Tris buffered saline solution supplemented with 10% donkey serum and 0.05% Triton-X (TBS-T) at 4^0C overnight. Tissues were incubated in 1:500 dilution of rat monoclonal MLKL antibody (clone 5A6, WEHI inhouse) at 4^0C overnight. Tissues were then washed in TBS-T and incubated in donkey anti-rat fluorochrome tagged secondary antibody 4^0C overnight. Finally tissues were washed gently in TBS-T followed by DAPI counterstain.

Quantification of mouse MLKL fluorescence of intensity

Random images were captured at 40X magnification. Intensity of MLKL was measured using Zen lite 3.3 edition by choosing the region of interest (ROI). ROI's were drawn around the airways and macrophages to measure the MLKL intensity in airway epithelial cells and alveolar macrophages, respectively.

Immunofluorescence staining for active caspase-3

As described for TUNEL assays, xylene was used to dewax and a graded ethanol series used to rehydrate paraffin-embedded mouse lung sections for histology. Following these steps antigen retrieval was performed by incubating tissues in citrate buffer (5% citric acid, 1.2% glacial acetic acid, 7.24% sodium acetate, and 3.4% sodium hydroxide, pH 6.0, 45 minutes, 100^0C) (14), followed by permeabilization with 0.5% Triton and 3% BSA in PBS (20 minutes, room temperature). Samples were blocked with 5% donkey serum for 1 hour. After three washes in PBS with 0.05% Tween-20 (PBS-T, 5 minutes each), samples were incubated with polyclonal primary antibody of active caspase-3 antibody (100 µL, 5 µg/ml, 4 ^{0}C, overnight, R&D Systems, AF835) in a humidified chamber. On the next day, after three PBS-T immersions, slices were immersed in secondary antibody Cy™3 AffiniPure F(ab')$_2$ Fragment Donkey Anti-Rabbit IgG (100 µL, H+L, Jackson ImmunoResearch, 711-166-152, 1:400 dilution with 0.05 % Triton and 0.3 % BSA in PBS, 60 minutes, room temperature). Control

AJRCCM Articles in Press. Published June 16, 2021 as 10.1164/rccm.202009-3442OC

slides were subjected to identical staining procedures but the primary antibody was omitted. Samples were washed and stained with Hoechst 33342. After mounting with coverslips, photos of 15 random views from each sample were taken and counted for the number of active caspase-3 positive signals relative to the total number of cells determined by the number of Hoechst-stained nuclei.

RNA extraction from mouse lung tissue

Whole lung tissue that had been stored at -80 ^{0}C was defrosted then homogenized using a Tissue-tearor stick homogeniser (BioSpec Products, USA) in TRIzol (1 mL, Life Technology) on ice (not exceeding 10 seconds per cycle to prevent sample overheating). Homogenates were transferred to fresh 1.5 mL tubes and centrifuged (12,000x*g*, 10 minutes, 4^{0}C). Supernatants were transferred to other fresh tubes and 250 µL chloroform (4^{0}C, Sigma-Aldrich, C2432) added for every 1 mL homogenate prior to pulse vortexing. After incubation (10 minutes, room temperature), another centrifugation (12,000x*g*, 10 minutes, 4^{0}C) was performed. The upper clear aqueous phase was then carefully collected (avoiding precipitated DNA at the interphase of the upper and lower phase), transferred into fresh tubes and RNA precipitated by adding ice-cold isopropanol (500 µL, Sigma-Aldrich, I9516) for every 1 mL homogenate. Samples were vortexed, incubated (10 minutes, room temperature), vortexed again and then centrifuged (12,000x*g*, 10 minutes, 4^{0}C). Supernatants were removed and RNA pellets washed with ethanol (75%, 1 mL ice-cold) and centrifuged (8,000x*g*, 7 minutes, 4^{0}C). Wash and centrifugation steps were repeated, ethanol carefully removed and RNA pellets air-dried (15 minutes), resuspended in nuclease-free water (nf-H_2O, 100 µL, Life Technologies, 10977-023) and stored (-20 ^{0}C).

Reverse transcription PCR (RT-PCR)

The concentration and quality of extracted RNA were determined using a NanoDrop spectrophotometer (Thermo Fisher Scientific). Bioscript^{TM} Kit (Bioline) and random hexamer

AJRCCM Articles in Press. Published June 16, 2021 as 10.1164/rccm.202009-3442OC

primers (Invitrogen) were used to perform reverse transcription. For each RT-PCR reaction RNA (1 μg) was diluted in nf-H_2O (into a total volume of 8 μL). DNAse I Mix (2 μL) was added (1 μL, 10X DNAse Reaction Buffer, 1 μL, DNase I 'amplification grade', Sigma-Aldrich, AMPD1) prior to incubation (15 minutes, room temperature) in 200 μL tubes. DNAse I Stop Solution (1 μL) was added to halt the DNAse reaction and samples were placed into a thermal cycler (Bio-Rad T100TM). Following heating (10 minutes, 65^0C), Random Primers/dNTP Mix (3 uL; 2 μL hexamers at 50 ng/μL and 1 μL at 10 mM dNTPs, Bioline, Bi 005) was added to each sample. Samples were then incubated (5 minutes, 65^0C and 10 minutes, 25^0C). Bioscript^{tm} MasterMix (4 μL 5X Reaction Buffer, 100 mM DTT, 1 μL nf-H_2O and 1 μL BioScript^{tm}) was added to each sample. Samples were further incubated (10 minutes at 25^0C, 50 minutes at 42^0C and 15 minutes at 70^0C). The resulting cDNA samples were diluted in 79 μL nf-H_2O and stored at -20 ^{0}C.

Quantitative PCR (qPCR)

Gene expression was assessed relative to a housekeeping gene (*Hprt* or *β-actin*) using a Viia™ 7 Real-time PCR machine (Life Technologies). Primers were self-designed (PCR product size 70-150 bp, primer melting temperatures (T_m) 55^0C to 65^0C, max T_m difference is 1^0C, no potential hairpin formation, no 3' complementarity nor potential self-annealing sites) and ordered from Integrated DNA Technologies (IDT). Primer sequences were:

Cxcl1	Forward primer	5′- GCTGGGATTCACCTCAAGAA -3′
	Reverse primer	5′- CTTGGGGACACCTTTTAGCA -3′
Mmp8	Forward primer	5′- GATTCAGAAGAAACGTGGACTCAA -3′
	Reverse primer	5′- CATCAAGGCACCAGGATCAGT-3′
Mmp12	Forward primer	5′- AGAGCAGTGCCCCAG AGGTCA -3′

AJRCCM Articles in Press. Published June 16, 2021 as 10.1164/rccm.202009-3442OC

	Reverse primer	5′- TCCTCACGCTTCATGTCCGGAG-3′
Mip1α	Forward primer	5'-CTCCCAGCCAGGTGTCATTTT-3'
	Reverse primer	5'-CTTGGACCCAGGTCTCTTTGG-3'
Ym1	Forward primer	5′- CCCCAGGAAGTACCCTATGCCT-3′
	Reverse primer	5′- AACCACTGAAGTCATCCATGTCC -3′
Marco	Forward primer	5′- GCACTGCTGCTGATTCAAGTTC -3′
	Reverse primer	5′- AGTTGCTCCTGGCTGGTATG -3′
Mlkl	Forward primer	5′- CCGGACAGCAAAGAGCACTA -3′
	Reverse primer	5′- TCTCCAAGATTCCGTCCACAG -3′
Ripk1	Forward primer	5′- TGACTTTCACATTAAGATAGCCGAT -3′
	Reverse primer	5′- TGTTCGGGTGCCATGTAGTA -3′
Ripk3	Forward primer	5′- AAGTTATGGCCTACTGGTGCG -3′
	Reverse primer	5′- TCCGAACCCTCCTTTACCCA -3′
Hsp90aa1	Forward primer	5′- AATTCATCGGACGCTCTGGA -3′
	Reverse primer	5′- TCCACAATGGTCAGGGTTCG -3′

For each sample, cDNA (2 µL), forward primer (0.5 µL 100 µM), reverse primer (0.5 µL 100 µM), nf-H_2O (4 µL), SYBR green (3 µL, Geneworks, KP-KK4602) and were mixed. Cycle settings were 50^0C 2 minutes, 95^0C 2 minutes, 40X (95^0C 15 seconds plus 60^0C 30 seconds), 95^0C 15 seconds, 60^0C 15 seconds, 8 minutes for dissociation curve, 95^0C 15 seconds.

Sorting of alveolar macrophages from BALF

Sorting of alveolar macrophages from BALF of mice exposed whole-body to air or cigarette smoke was performed using a FACS Aria (BD Biosciences, Franklin Lakes, NJ, USA) (27). To minimize non-specific binding, BAL cells were first incubated with FcR blocking antibody

AJRCCM Articles in Press. Published June 16, 2021 as 10.1164/rccm.202009-3442OC

(anti-CD16/CD32, clone 2.4G2). Afterwards, labelling reactions were performed to identify macrophages. The following antibodies were used: FITC conjugated CD45 (30-F11), PE conjugated Siglec-F (E50-2440) and APC conjugated CD11c (HL3) from BD Biosciences. As a first step, doublets were excluded, live cells were gated as FVD eFluor™ 506- and $CD45^+$ cells were retained. Macrophages were then gated as $SiglecF^+$ and $CD11c^+$.

RNA sequencing of FACS sorted mouse alveolar macrophages and data processing

PolyA+ RNA sequencing libraries were prepared using the TruSeq mRNA library prep kit (Illumina, San Diego, CA, USA) according to the manufacturer's instructions. A total of 25 ng of RNA was used as input for polyA selection, followed by fragmentation, reverse transcription and PCR amplification. Libraries were quantified and pooled for single-end sequencing on an Illumina NextSeq 500 system. Poly-A RNA-sequencing reads were mapped to the murine reference genome (GRCm38.p6) using STAR v2.6.0c (28) and GENCODE release M18 as guidance, resulting in 80.7 ± 5.6% (mean ± sd) uniquely mapped reads. Read counts were finally quantified using the "--quantMode GeneCounts" option from STAR. Genomic features with a zero read count across all samples and without a read count >4 in at least 60% of the samples from one group were discarded. Normalization, log2-transformation into counts per million (logCPM) and differential gene expression analyses were performed using the R statistical programming language (version 3.5.1) and the limma package (version 3.38.2)(29). Genes showing log2 fold-change and differences >1 (in absolute value) between the different pairwise comparisons and with Benjamini-Hochberg adjusted p-values <0.05 were considered differentially expressed. This data set has been uploaded to NCBI GEO (ID: GSE137653) (27).

Protein extraction from mouse lung tissue

Whole lung tissue that had been stored at -80 ^{0}C was homogenized using a Tissue-tearor stick homogeniser (BioSpec Products, USA) in lysis buffer (200 µL, 150 mM NaCl, 20 mM Tris

AJRCCM Articles in Press. Published June 16, 2021 as 10.1164/rccm.202009-3442OC

pH7.5, 1 mM EDTA, 1mM EGTA, 1 % Triton X-100, 10 mM NaF). Phosphatase and protease inhibitor cocktails (Roche, PhosSTOP™, cOmplete™) were added to lysis buffer immediately before use. Once homogenized, samples were incubated (15 minutes on ice) then centrifuged (10,000x*g*, 10 minutes, 4^0C) and supernatants collected. Protein concentrations were measured using bicinchoninic acid (BCA) Assays (Thermo Scientific) according to the manufacturer's instructions. Albumin (BSA) standard (2 mg/mL) was diluted to 8 concentrations from 25 to 2000 μg/mL to make a standard curve in a 96 well plate, at the same time the samples were added. After incubation (30 minutes, 37^0C) with the working reagent (0.2% cupric sulfate, sodium carbonate, sodium bicarbonate, bicinchoninic acid and sodium tartrate in 0.1M sodium hydroxide) absorbance at 562 nm was read on a plate reader (BMG LABTECH, FLUOstar OPTIMA). Sample protein concentrations were calculated according to the BSA standard curve. Quantified protein samples were stored at -80^0C.

SDS-PAGE and immunoblot of mouse samples

Polyacrylamide gel electrophoresis (SDS-PAGE) was performed using 4–15% Mini-PROTEAN™ TGX Stain-Free™ Protein Gels (Bio-Rad, 4568086). For each sample, protein (30 μg) was diluted into 1X Laemmli Sample Buffer (Bio-Rad, 1610747) and heated (5 minutes, 100^0C). Samples were then loaded into wells and proteins separated by applying an electrical current (110 V, 90 minutes) to the gel, which was immersed in SDS-PAGE running buffer (24 mM Tris, 0.192 M glycine, 0.1% SDS pH 8.3). Once separation was complete, proteins were transferred to Immobilon-P Membrane (PVDF membrane, Merck Millipore, IPVH00010) using a large semi-dry transfer unit ((30 V, 60 minutes, Hoefer TE77XP). Towbin transfer buffer (192 mM Glycine, 25 mM SDS, 20% Methanol) was used for transfer. Membranes with transferred protein were exposed to 5% milk powder in TBS-T (120 mM NaCl, 10 mM Tris, pH 8.0) for blocking (4^0C, overnight), then washed with TBS-T (5 minutes,

AJRCCM Articles in Press. Published June 16, 2021 as 10.1164/rccm.202009-3442OC

four times). Primary antibodies used were: purified mouse anti-*Ripk1* (1:2,000, BD Transduction Laboratories™, cat# 610459), rabbit anti-*Ripk3* (1:2,000, Enzo Life Sciences, cat# ADI-905-242), anti-MLKL antibody - C-terminal (1:1,000, Abcam, ab172868). All antibodies (primary and secondary) were diluted in TBS-T. After incubation with primary antibodies (1 hour, room temperature), membranes were washed with TBS-T (5 minutes, four times). Secondary antibodies were anti-mouse/rabbit IgG (1:3,000, 1 hour at room temperature, Cell Signaling Technology). After further TBS-T washes (5 minutes, four times) SuperSignal West Femto Maximum Sensitivity Substrate (Thermo Scientific) was added to membranes and incubated (2 minutes). A ChemiDoc™ (Bio-Rad Laboratories) was used to detect chemiluminescent signals and analysis of membrane images. A protein molecular weight marker was included in all gels (Precision Plus Protein™ WesternC™ Pack, Bio-Rad Laboratories cat# 161-0385, 3 µL standard with 1:20,000 StrepTactin-HRP conjugate).

Histopathology

Hematoxylin and eosin (H&E) stained mouse lung sections were prepared by the Imaging and Cytometry Facility at Australian National University, Canberra, and histopathology of airways, vasculature and parenchyma assessed. Airways and vascular histopathological changes were quantified as previously described (30) using the following:

Airway inflammation score
0= airway has no surrounding inflammatory cells
1= airway has minor inflammatory cells around
2= airway has intermediate inflammatory cells around
3= airway has massive inflammatory cells around or complete surround
Vasculature

AJRCCM Articles in Press. Published June 16, 2021 as 10.1164/rccm.202009-3442OC

0= blood vessel has no surrounding inflammatory cells
1= blood vessel has minor inflammatory cells around
2= blood vessel has intermediate inflammatory cells around
3= blood vessel has massive inflammatory cells around or complete surround

The average scores for each slide were pooled for statistical analyses.

Parenchymal macrophage count

Fifteen random fields (40X) of parenchymal tissue of H&E-stained lung slices were imaged (fields with airways or large blood vessels were excluded). Macrophages were distinguished by morphology, and their numbers in images were recorded as average macrophage numbers per view.

Airway remodelling

Lungs were perfused with 0.9% saline under the pressure of 30 cm H_2O for 60 seconds to remove blood from lung vessels. Tracheas were cannulated and lungs gently inflated with and then submerged in 10% buffered formalin (1 mL). Fixed volume inflation was used as it maintains lung architecture and prevents over-inflation that would artificially increase alveolar size in mice with emphysema (7, 31). Lungs were fixed and embedded in paraffin, and 5 μm sections were stained with Sirius Red and Fast Green (Imaging and Cytometry Facility, ANU, Canberra) to enable visualization of collagen fibres in lung tissue. All complete small airways (Pbm <1,000 μm) were recorded (at 40X magnification) and area of stained collagen analysed using Image J. Color deconvolution was performed to allow selective analysis of the collagen signal (14). Morphometric parameters were manually selected and used to measure area of airway epithelia that were normalized to the Pbm. Collagen area was measured and normalized

AJRCCM Articles in Press. Published June 16, 2021 as 10.1164/rccm.202009-3442OC

to the Pbm.

Mean linear intercept (MLI)-based quantification of emphysema-like alveolar enlargement

Fifteen random fields (40X) of parenchymal tissue of H&E-stained lung sections were imaged (fields with airways or large blood vessels were excluded) using a light microscope (BX41, Olympus, Japan) and ImagePro Plus software (version 7). MLI counts were performed on the images (14). An MLI mask with 11 evenly spaced horizontal lines was overlaid onto random fields. The number of intercepts between the parenchymal tissue and the horizontal lines was recorded. The MLI of each overlaid image equates to 3832.2141 μm over the number of intercepts. The average number of 15 random fields was recorded as the MLI.

AJRCCM Articles in Press. Published June 16, 2021 as 10.1164/rccm.202009-3442OC

References

1. Maes T, Bracke KR, Vermaelen KY, Demedts IK, Joos GF, Pauwels RA, Brusselle GG. Murine TLR4 is implicated in cigarette smoke-induced pulmonary inflammation. *Int Arch Allergy Immunol* 2006; 141: 354-368.

2. Bracke KR, Verhamme FM, Seys LJ, Bantsimba-Malanda C, Cunoosamy DM, Herbst R, Hammad H, Lambrecht BN, Joos GF, Brusselle GG. Role of CXCL13 in cigarette smoke-induced lymphoid follicle formation and chronic obstructive pulmonary disease. *Am J Respir Crit Care Med* 2013; 188: 343-355.

3. Verhamme FM, De Smet EG, Van Hooste W, Delanghe J, Verleden SE, Joos GF, Brusselle GG, Bracke KR. Bone morphogenetic protein 6 (BMP-6) modulates lung function, pulmonary iron levels and cigarette smoke-induced inflammation. *Mucosal Immunol* 2019; 12: 340-351.

4. Murphy JM, Czabotar PE, Hildebrand JM, Lucet IS, Zhang JG, Alvarez-Diaz S, Lewis R, Lalaoui N, Metcalf D, Webb AI, Young SN, Varghese LN, Tannahill GM, Hatchell EC, Majewski IJ, Okamoto T, Dobson RC, Hilton DJ, Babon JJ, Nicola NA, Strasser A, Silke J, Alexander WS. The pseudokinase MLKL mediates necroptosis via a molecular switch mechanism. *Immunity* 2013; 39: 443-453.

5. Newton K, Sun X, Dixit VM. Kinase RIP3 is dispensable for normal NF-kappa Bs, signaling by the B-cell and T-cell receptors, tumor necrosis factor receptor 1, and Toll-like receptors 2 and 4. *Mol Cell Biol* 2004; 24: 1464-1469.

6. Rickard JA, O'Donnell JA, Evans JM, Lalaoui N, Poh AR, Rogers T, Vince JE, Lawlor KE, Ninnis RL, Anderton H, Hall C, Spall SK, Phesse TJ, Abud HE, Cengia LH, Corbin J, Mifsud S, Di Rago L, Metcalf D, Ernst M, Dewson G, Roberts AW,

AJRCCM Articles in Press. Published June 16, 2021 as 10.1164/rccm.202009-3442OC

Alexander WS, Murphy JM, Ekert PG, Masters SL, Vaux DL, Croker BA, Gerlic M, Silke J. RIPK1 regulates RIPK3-MLKL-driven systemic inflammation and emergency hematopoiesis. *Cell* 2014; 157: 1175-1188.

7. Beckett EL, Stevens RL, Jarnicki AG, Kim RY, Hanish I, Hansbro NG, Deane A, Keely S, Horvat JC, Yang M, Oliver BG, van Rooijen N, Inman MD, Adachi R, Soberman RJ, Hamadi S, Wark PA, Foster PS, Hansbro PM. A new short-term mouse model of chronic obstructive pulmonary disease identifies a role for mast cell tryptase in pathogenesis. *J Allergy Clin Immunol* 2013; 131: 752-762.

8. Hansbro PM, Hamilton MJ, Fricker M, Gellatly SL, Jarnicki AG, Zheng D, Frei SM, Wong GW, Hamadi S, Zhou S, Foster PS, Krilis SA, Stevens RL. Importance of mast cell Prss31/transmembrane tryptase/tryptase-gamma in lung function and experimental chronic obstructive pulmonary disease and colitis. *J Biol Chem* 2014; 289: 18214-18227.

9. Fricker M, Deane A, Hansbro PM. Animal models of chronic obstructive pulmonary disease. *Expert opinion on drug discovery* 2014; 9: 629-645.

10. Vlahos R, Bozinovski S. Recent advances in pre-clinical mouse models of COPD. *Clin Sci (Lond)* 2014; 126: 253-265.

11. Hsu AC, Starkey MR, Hanish I, Parsons K, Haw TJ, Howland LJ, Barr I, Mahony JB, Foster PS, Knight DA, Wark PA, Hansbro PM. Targeting PI3K-p110alpha Suppresses Influenza Virus Infection in Chronic Obstructive Pulmonary Disease. *Am J Respir Crit Care Med* 2015; 191: 1012-1023.

12. Tay HL, Kaiko GE, Plank M, Li J, Maltby S, Essilfie AT, Jarnicki A, Yang M, Mattes J, Hansbro PM, Foster PS. Antagonism of miR-328 increases the antimicrobial function

AJRCCM Articles in Press. Published June 16, 2021 as 10.1164/rccm.202009-3442OC

of macrophages and neutrophils and rapid clearance of non-typeable Haemophilus influenzae (NTHi) from infected lung. *PLoS Pathog* 2015; 11: e1004549.

13. Thorburn AN, Tseng HY, Donovan C, Hansbro NG, Jarnicki AG, Foster PS, Gibson PG, Hansbro PM. TLR2, TLR4 AND MyD88 Mediate Allergic Airway Disease (AAD) and Streptococcus pneumoniae-Induced Suppression of AAD. *PLoS One* 2016; 11: e0156402.

14. Liu G, Cooley MA, Jarnicki AG, Hsu AC, Nair PM, Haw TJ, Fricker M, Gellatly SL, Kim RY, Inman MD, Tjin G, Wark PA, Walker MM, Horvat JC, Oliver BG, Argraves WS, Knight DA, Burgess JK, Hansbro PM. Fibulin-1 regulates the pathogenesis of tissue remodeling in respiratory diseases. *JCI Insight* 2016; 1.

15. Jarnicki AG, Schilter H, Liu G, Wheeldon K, Essilfie AT, Foot JS, Yow TT, Jarolimek W, Hansbro PM. The inhibitor of semicarbazide-sensitive amine oxidase, PXS-4728A, ameliorates key features of chronic obstructive pulmonary disease in a mouse model. *Br J Pharmacol* 2016; 173: 3161-3175.

16. Conickx G, Mestdagh P, Avila Cobos F, Verhamme FM, Maes T, Vanaudenaerde BM, Seys LJ, Lahousse L, Kim RY, Hsu AC, Wark PA, Hansbro PM, Joos GF, Vandesompele J, Bracke KR, Brusselle GG. MicroRNA Profiling Reveals a Role for MicroRNA-218-5p in the Pathogenesis of Chronic Obstructive Pulmonary Disease. *Am J Respir Crit Care Med* 2017; 195: 43-56.

17. Hsu AC, Dua K, Starkey MR, Haw TJ, Nair PM, Nichol K, Zammit N, Grey ST, Baines KJ, Foster PS, Hansbro PM, Wark PA. MicroRNA-125a and -b inhibit A20 and MAVS to promote inflammation and impair antiviral response in COPD. *JCI Insight* 2017; 2: e90443.

AJRCCM Articles in Press. Published June 16, 2021 as 10.1164/rccm.202009-3442OC

18. Starkey MR, Plank MW, Casolari P, Papi A, Pavlidis S, Guo Y, Cameron GJM, Haw TJ, Tam A, Obiedat M, Donovan C, Hansbro NG, Nguyen DH, Nair PM, Kim RY, Horvat JC, Kaiko GE, Durum SK, Wark PA, Sin DD, Caramori G, Adcock IM, Foster PS, Hansbro PM. IL-22 and its receptors are increased in human and experimental COPD and contribute to pathogenesis. *Eur Respir J* 2019; 54.

19. D'Hulst A I, Vermaelen KY, Brusselle GG, Joos GF, Pauwels RA. Time course of cigarette smoke-induced pulmonary inflammation in mice. *Eur Respir J* 2005; 26: 204-213.

20. Bracke KR, D'Hulst A I, Maes T, Moerloose KB, Demedts IK, Lebecque S, Joos GF, Brusselle GG. Cigarette smoke-induced pulmonary inflammation and emphysema are attenuated in CCR6-deficient mice. *J Immunol* 2006; 177: 4350-4359.

21. Seys LJ, Verhamme FM, Schinwald A, Hammad H, Cunoosamy DM, Bantsimba-Malanda C, Sabirsh A, McCall E, Flavell L, Herbst R, Provoost S, Lambrecht BN, Joos GF, Brusselle GG, Bracke KR. Role of B Cell-Activating Factor in Chronic Obstructive Pulmonary Disease. *Am J Respir Crit Care Med* 2015; 192: 706-718.

22. Clauss M, Voswinckel R, Rajashekhar G, Sigua NL, Fehrenbach H, Rush NI, Schweitzer KS, Yildirim AO, Kamocki K, Fisher AJ, Gu Y, Safadi B, Nikam S, Hubbard WC, Tuder RM, Twigg HL, 3rd, Presson RG, Sethi S, Petrache I. Lung endothelial monocyte-activating protein 2 is a mediator of cigarette smoke-induced emphysema in mice. *J Clin Invest* 2011; 121: 2470-2479.

23. Haw TJ, Starkey MR, Nair PM, Pavlidis S, Liu G, Nguyen DH, Hsu AC, Hanish I, Kim RY, Collison AM, Inman MD, Wark PA, Foster PS, Knight DA, Mattes J, Yagita H, Adcock IM, Horvat JC, Hansbro PM. A pathogenic role for tumor necrosis factor-

AJRCCM Articles in Press. Published June 16, 2021 as 10.1164/rccm.202009-3442OC

related apoptosis-inducing ligand in chronic obstructive pulmonary disease. *Mucosal Immunol* 2016; 9: 859-872.

24. Starkey MR, Nguyen DH, Brown AC, Essilfie AT, Kim RY, Yagita H, Horvat JC, Hansbro PM. Programmed Death Ligand 1 Promotes Early-Life Chlamydia Respiratory Infection-Induced Severe Allergic Airway Disease. *Am J Respir Cell Mol Biol* 2016; 54: 493-503.

25. Fricker M, Goggins BJ, Mateer S, Jones B, Kim RY, Gellatly SL, Jarnicki AG, Powell N, Oliver BG, Radford-Smith G, Talley NJ, Walker MM, Keely S, Hansbro PM. Chronic cigarette smoke exposure induces systemic hypoxia that drives intestinal dysfunction. *JCI Insight* 2018; 3.

26. Ding J, Lu Q, Ouyang Y, Mao H, Zhang P, Yao J, Xu C, Li X, Xiao J, Zhang Q. A long noncoding RNA regulates photoperiod-sensitive male sterility, an essential component of hybrid rice. *Proc Natl Acad Sci U S A* 2012; 109: 2654-2659.

27. De Smet EG, Van Eeckhoutte HP, Avila Cobos F, Blomme E, Verhamme FM, Provoost S, Verleden SE, Venken K, Maes T, Joos GF, Mestdagh P, Brusselle GG, Bracke KR. The role of miR-155 in cigarette smoke-induced pulmonary inflammation and COPD. *Mucosal Immunol* 2020; 13: 423-436.

28. Dobin A, Davis CA, Schlesinger F, Drenkow J, Zaleski C, Jha S, Batut P, Chaisson M, Gingeras TR. STAR: ultrafast universal RNA-seq aligner. *Bioinformatics* 2013; 29: 15-21.

29. Ritchie ME, Phipson B, Wu D, Hu Y, Law CW, Shi W, Smyth GK. limma powers differential expression analyses for RNA-sequencing and microarray studies. *Nucleic Acids Res* 2015; 43: e47.

AJRCCM Articles in Press. Published June 16, 2021 as 10.1164/rccm.202009-3442OC

30. Horvat JC, Beagley KW, Wade MA, Preston JA, Hansbro NG, Hickey DK, Kaiko GE, Gibson PG, Foster PS, Hansbro PM. Neonatal chlamydial infection induces mixed T-cell responses that drive allergic airway disease. *Am J Respir Crit Care Med* 2007; 176: 556-564.

31. Braber S, Verheijden KA, Henricks PA, Kraneveld AD, Folkerts G. A comparison of fixation methods on lung morphology in a murine model of emphysema. *American journal of physiology Lung cellular and molecular physiology* 2010; 299: L843-851.

AJRCCM Articles in Press. Published June 16, 2021 as 10.1164/rccm.202009-3442OC

Supplementary table E1 Characteristics of study subjects for RIPK3 and MLKL immunohistochemistry (n=48)

	never smokers	smokers without COPD	COPD GOLD II	COPD GOLD III-IV
Number	8	16	16	8
Age (years)	65 (62-77)	66 (57-70)	68 (62-69)	57 (52-59)*†§
Gender ratio (m/f)	3/5#	13/3#	13/3#	3/5#
Current- / ex-smoker	NA	8/8#	8/8#	0/8#
Pack-years	NA	26 (20-50)*	44 (34-56)*	40 (32-50)*
FEV_1 post (L)	2.4 (1.9-2.9)	2.8 (2.5-3.4)	2.0 (1.7-2.3)†	0.7 (0.4-1.0)*†§
FEV_1 post (% predicted)	96 (89-102)	99 (91-117)	68 (61-76)*†	24 (18-34)*†§
FEV_1/FVC post	81 (72-93)	77 (72-81)	56 (49-63)*†	28 (26-35)*†§
DL_{CO} (% predicted)	93 (78-102)	84 (64-101)	67 (50-83)*	33 (31-37)*†§
K_{CO} (% predicted)	110 (92-135)	96 (80-119)	80 (60-105)	51 (39-58)*†§
ICS (yes/no)	0/8#	0/16#	9/7#	8/0#

m (male); f (female); FEV_1 (forced expiratory volume in 1 second); FVC (forced vital capacity); DL_{CO} (diffusing capacity of the lungs for carbon monoxide); ICS (inhaled corticosteroids); NA (not applicable)

Data are presented as median (IQR)

Mann-Whitney U test: * $P < 0.05$ versus never smokers, † $P < 0.05$ versus smokers without COPD, § $P < 0.05$ versus COPD GOLD II. Fisher's exact test: # $P<0.001$.

AJRCCM Articles in Press. Published June 16, 2021 as 10.1164/rccm.202009-3442OC

Supplementary Table E2. Characteristics of study subjects for RIPK3, pRIPK3, MLKL and pMLKL immunoblot (n=40)

	never smokers	smokers without COPD	COPD GOLD II	COPD GOLD III-IV
Number	10	10	10	10
Age (years)	63 (38-70)	62 (56-71)	66 (57-69)	56 (54-59)
Gender ratio (m/f)	4/6	6/4	6/4	6/4
Current- / ex-smoker	NA	5/5[#]	6/4[#]	0/10[#]
Pack-years	NA	22 (14-39)[*]	41 (30-51)[*†]	30 (25-31)[*§]
FEV_1 post (L)	2.6 (2.1-4.2)	2.7 (2.2-3.4)	1.8 (1.4-2.1)[*†]	0.7 (0.6-0.8)[*†§]
FEV_1 post (% predicted)	110 (97-118)	108 (91-120)	63 (58-77)[*†]	23 (20-29)[*†§]
FEV_1/FVC post	80 (77-82)	77 (76-82)	53 (46-64)[*†]	32 (26-38)[*†§]
DL_{CO} (% predicted)	94 (81-108)	89 (84-109)	50 (44-59)[*†]	36 (33-41)[*†§]
K_{CO} (% predicted)	96 (84-117)	98 (91-119)	60 (52-83)[*†]	59 (50-65)[*†]
ICS (yes/no)	0/10[#]	0/10[#]	5/5[#]	9/1[#]

m (male); f (female); FEV_1 (forced expiratory volume in 1 second); FVC (forced vital capacity); DL_{CO} (diffusing capacity of the lungs for carbon monoxide); ICS (inhaled corticosteroids); NA (not applicable)

Data are presented as median (IQR)

Mann-Whitney U test: [*] $P < 0.05$ versus never smokers, [†] $P < 0.05$ versus smokers without COPD, [§] $P < 0.05$ versus COPD GOLD II. Fisher's exact test: [#] $P<0.001$.

AJRCCM Articles in Press. Published June 16, 2021 as 10.1164/rccm.202009-3442OC

Figure legends

Supplementary Figure E1. Immunohistochemistry for RIPK3 and immunoblot for RIPK3 and MLKL in clinical samples. Representative images of immunohistochemical staining for RIPK3 in lung tissue sections (*A*) from never smokers, smokers without airflow limitation, patients with COPD GOLD II and III-IV. (*B*) Quantification of RIPK3 positive staining in airway epithelium, n=8-16. (*C*) Immunoblot and (*D*) quantification of RIPK3 and (*E*, *F*) MLKL on lung tissue homogenates from never smokers, smokers without airflow limitation, patients with COPD GOLD II and III-IV, n=10 patients/group. (*G*, *H*) Quantification of pRIPK3 and pMLKL immunoblotting of human lung tissue homogenates, assessed by densitometry, with band intensities were normalized to total RIPK3 or total MLKL, n=9-10 patients/group. Outliers were detected using the ROUT-test (n=2) and excluded from the analysis in (*G*, *H*). Statistical analyses used are one-way ANOVA with Bonferroni *post-hoc* for multiple comparisons (*D*, *F*) or Kruskal-Wallis test with Dunn's multiple comparisons (*B*, *G-H*). Results are median ± IQR. IQR: Interquartile range, GAPDH: glyceraldehyde-3-phosphate dehydrogenase, DL_{CO}: diffusing lung capacity of carbon monoxide.

Supplementary Figure E2. *Ripk1* mRNA expression relative to *Hprt* after (*A*) 4, (*B*) 8 and (*C*) 12 weeks of nose-only cigarette smoke exposure. *Ripk3* mRNA expression relative to *Hprt* after (*D*) 4, (*E*) 8 and (*F*) 12 weeks, n=6/group. Quantification of mouse MLKL signal intensity in airway epithelium (*G*) and macrophages (H) of mice exposed to 8 weeks of air- or CS (nose-only), n=3/group. Data are mean ± SEM. # compared to WT air-exposed controls. # = $P<0.05$, Student's *t-test*.

Supplementary Figure E3. Levels of whole lung mRNA expression after acute CS exposure (1-week nose-only) of (*A*) *Cxcl1*, (*B*) *Mmp8*, (*C*) *Mmp12*, (*D*) *Ym1*, (*E*) *Marco*, (*F*) *Mip1a* and (*G*) *Ripk3* in WT air- and CS-exposed WT and *Ripk3*$^{-/-}$ mice， n=3-6/group. Levels of mRNA

AJRCCM Articles in Press. Published June 16, 2021 as 10.1164/rccm.202009-3442OC

expression of (*H*) *Cxcl1*, (*I*) *Mmp8*, (*J*) *Mmp12*, (*K*) *Ym1*, (*L*) *Marco*, (*M*) *Mip1a* and (*N*) *Mlkl* in air- and CS-exposed WT and *Mlkl*$^{-/-}$ mice， n=5-6/group. Data are mean ± SEM. * compared to other groups indicated. * = P<0.05, ** = P<0.01, **** = P<0.0001. # compared to WT air-exposed controls. # = P<0.05, ## = P<0.01, #### = P<0.0001. One-way ANOVA with Bonferroni correction for multiple comparisons was used.

Supplementary Figure E4. Levels of whole lung mRNA expression in experimental COPD (8-weeks nose-only CS exposure) of (*A*) *Cxcl1*, (*B*) *Mmp8*, (*C*) *Mmp12*, (*D*) *Ym1*, (*E*) *Marco*, (*F*) *Mip1a* and (*G*) *Ripk3* in air- and CS-exposed WT and *Ripk3*$^{-/-}$ mice. Data are mean ± SEM of n=5-6/group. * compared to other groups indicated. * = P<0.05, **** = P<0.0001. # compared to WT air-exposed controls. # = P<0.05, ## = P<0.01, #### = P<0.0001. One-way ANOVA with Bonferroni correction for multiple comparisons was used.

Supplementary Figure E5. Levels of whole lung mRNA expression in experimental COPD (8-weeks nose-only CS exposure) of (*A*) *Cxcl1*, (*B*) *Mmp8*, (*C*) *Mmp12*, (*D*) *Ym1*, (*E*) *Marco*, (*F*) *Mip1a* and (*G*) *Mlkl* in air- and CS-exposed WT and *Mlkl*$^{-/-}$ mice with or without qVD-OPh treatment. Data are mean ± SEM of n=6/group. * compared to other groups indicated. * = P<0.05, ** = P<0.01, **** = P<0.0001. # compared to WT air-exposed controls. # = P<0.05, ## = P<0.01, ### = P<0.001, #### = P<0.0001. One-way ANOVA with Bonferroni correction for multiple comparisons was used.

Supplementary Figure E6. Levels of mRNA expression of (A) *Cxcl1*, (B) *Mmp8*, (C) *Mmp12*, (D) *Ym1*, (E) *Marco* and (F) *Mip1α mRNA* expression in alveolar macrophages sorted by flow cytometry from BALF of mice exposed to whole body CS for 4 weeks. Data are mean ± SEM of n=5 mice/ group. # compared to WT air-exposed controls. # = P<0.05, ## = P<0.01, ### = P<0.001, Student's *t-test* was used.

AJRCCM Articles in Press. Published June 16, 2021 as 10.1164/rccm.202009-3442OC

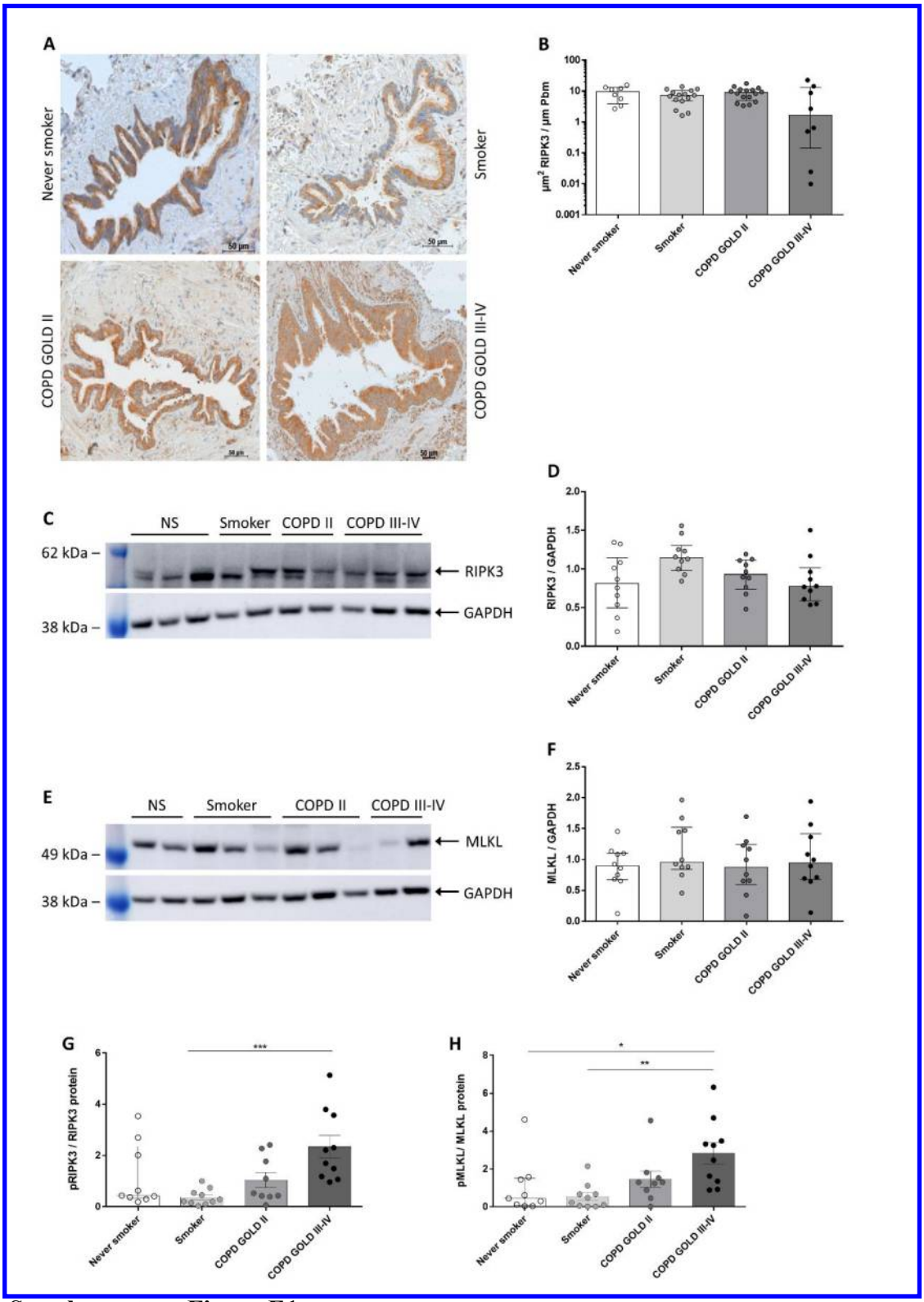

Supplementary Figure E1

AJRCCM Articles in Press. Published June 16, 2021 as 10.1164/rccm.202009-3442OC

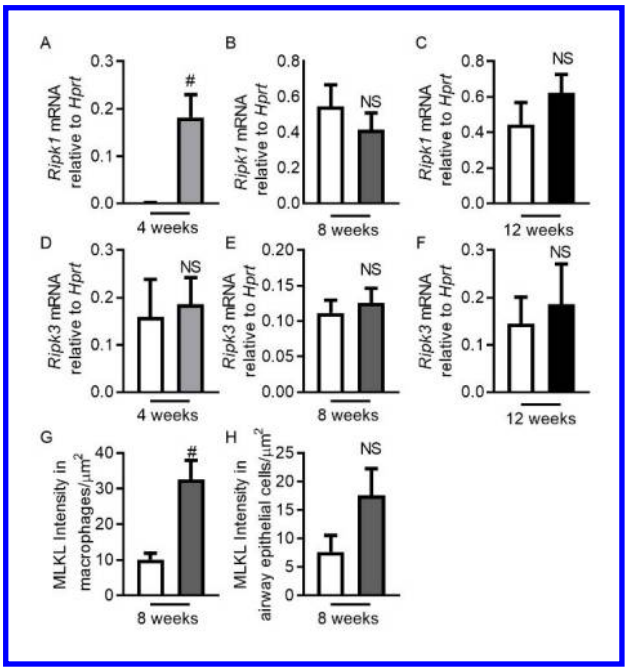

Supplementary Figure E2

AJRCCM Articles in Press. Published June 16, 2021 as 10.1164/rccm.202009-3442OC

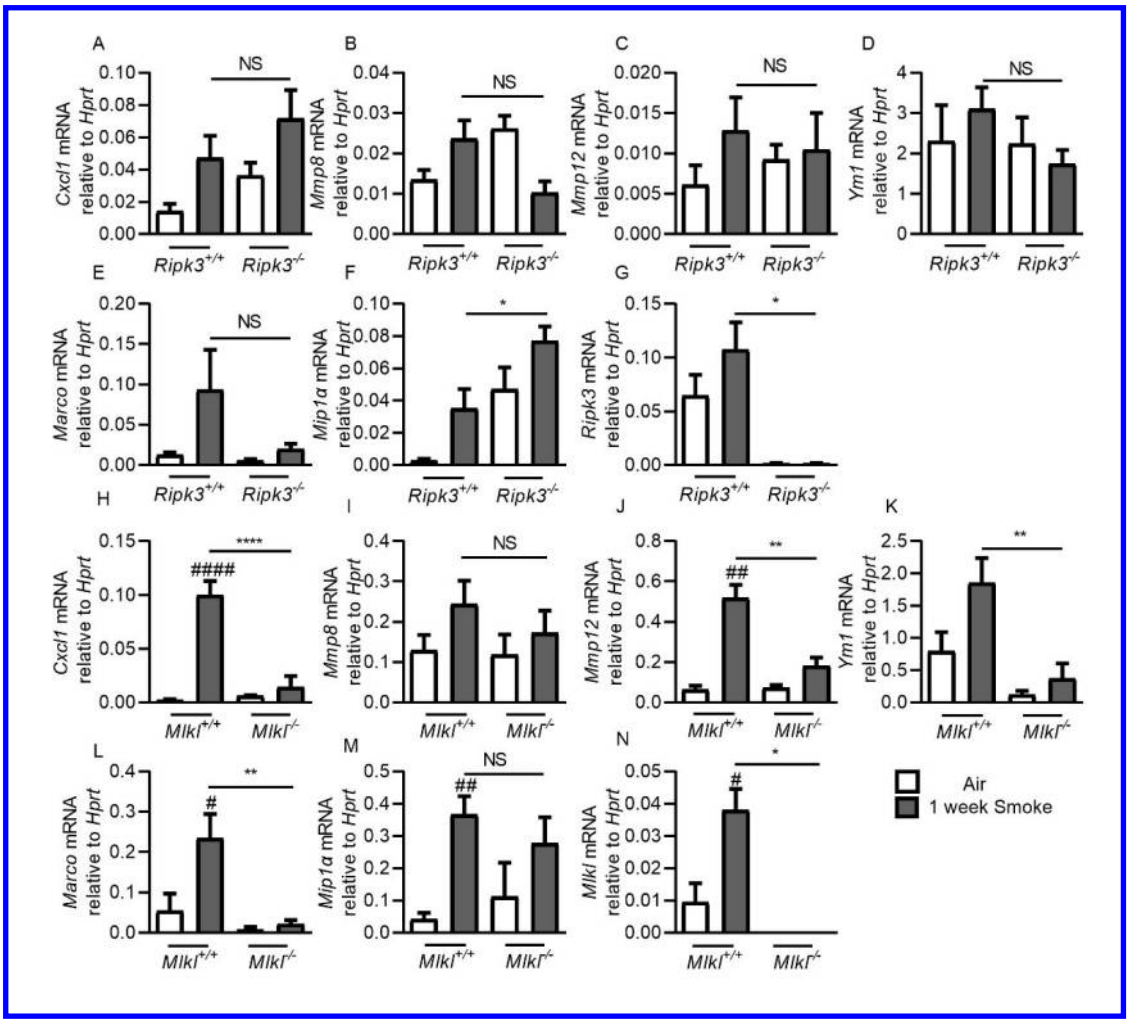

Supplementary Figure E3

AJRCCM Articles in Press. Published June 16, 2021 as 10.1164/rccm.202009-3442OC

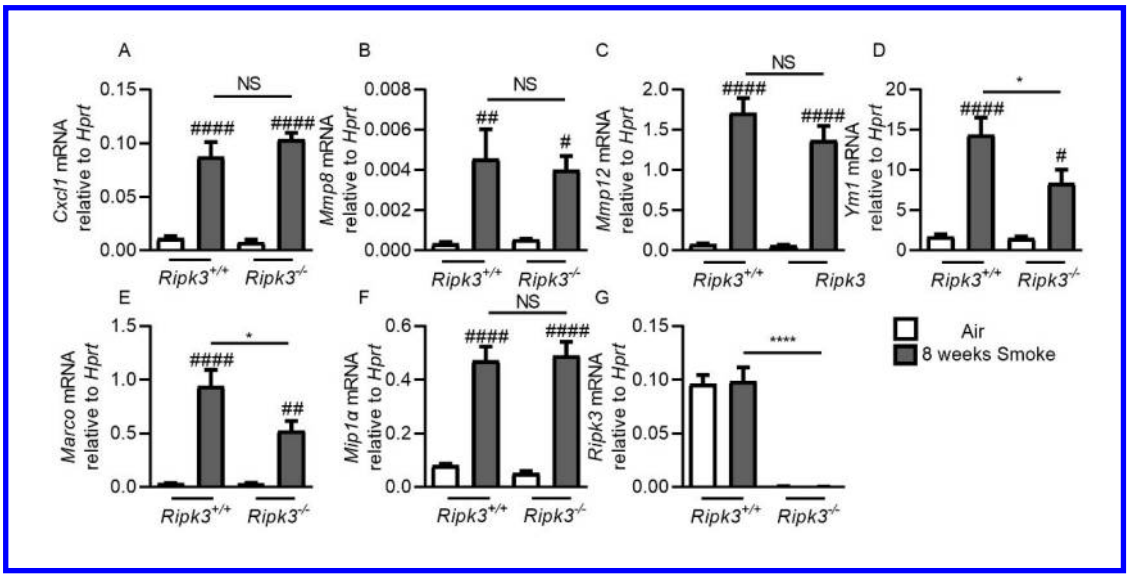

Supplementary Figure E4

AJRCCM Articles in Press. Published June 16, 2021 as 10.1164/rccm.202009-3442OC

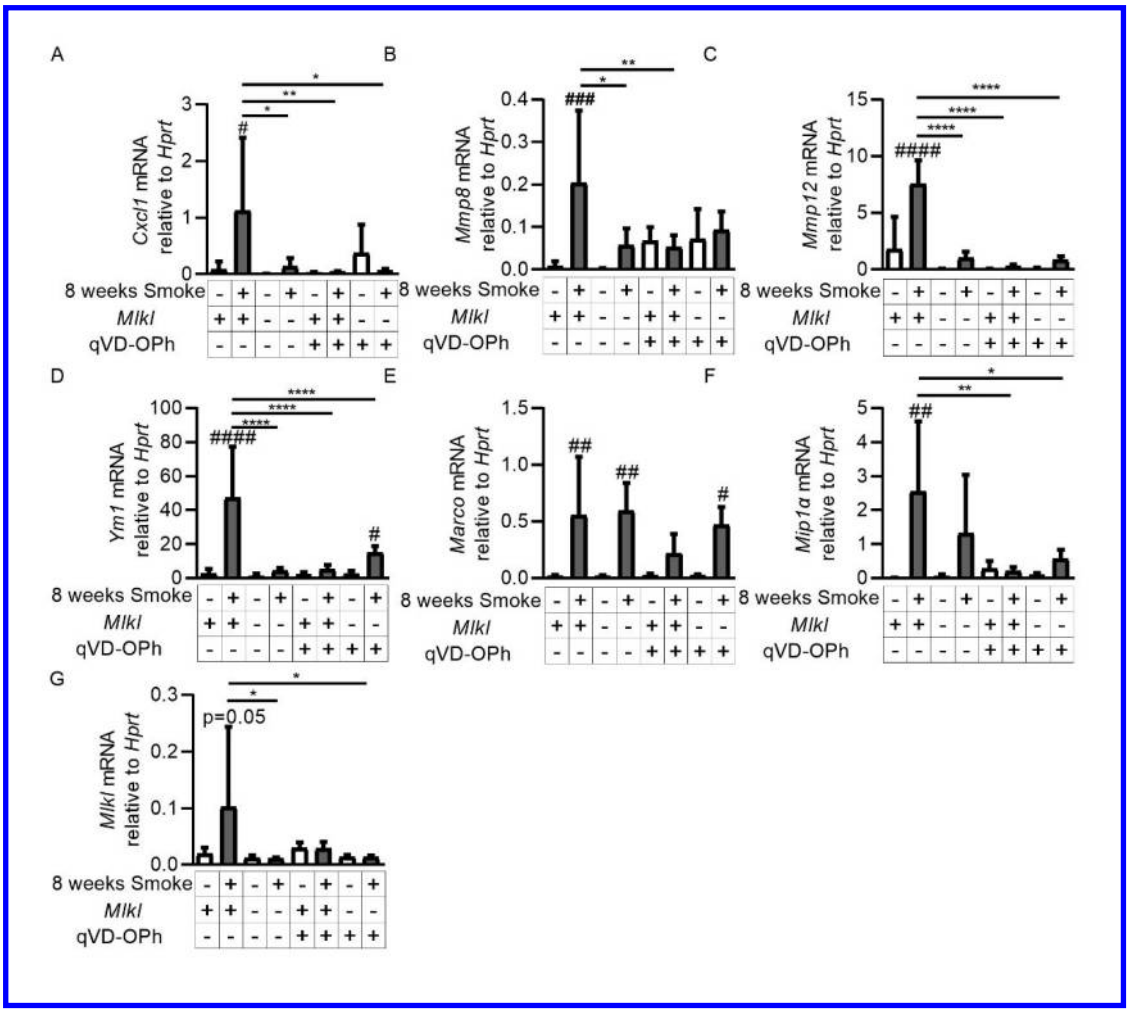

Supplementary Figure E5

AJRCCM Articles in Press. Published June 16, 2021 as 10.1164/rccm.202009-3442OC

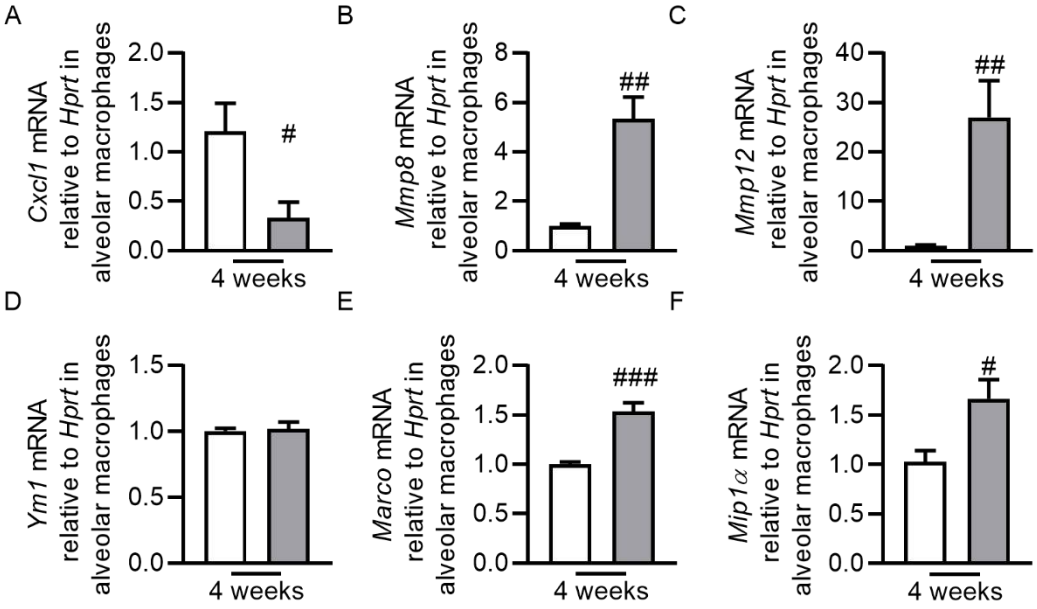

Supplementary Figure E6

AJRCCM Articles in Press. Published June 16, 2021 as 10.1164/rccm.202009-3442OC